Orientation of graphene nano sheets in magnetic fields

Progress in Materials Science 143 (2024) 101251

Contents lists available at ScienceDirect

Progress in Materials Science

journal homepage: www.elsevier.com/locate/pmatsci

Orientation of graphene nanosheets in magnetic fields

Viney Ghai [*], Sajjad Pashazadeh [1], Hengzhi Ruan [1], Roland Kádár [*]

Chalmers University of Technology, Industrial and Materials Science, 41296 Göteborg, Sweden

ARTICLE INFO

Keywords:
Graphene
Magnetic fields
Orientation

ABSTRACT

Aligning anisotropic nanoparticles using external fields is one of the major obstacles to unlocking their enormous potential for novel applications. The most famous such example is graphene, a 2D family of nanomaterials that has received enormous attention since its discovery. Using graphene to enhance mechanical, thermal, electric or gas barrier properties, imparting antibacterial properties etc., relies to a great extent on the ability to control their orientation inside a matrix material, i.e., polymers. Here we summarize the latest advances on graphene orientation using magnetic fields. The review covers the underlying physics for graphene interaction with magnetic fields, theoretical continuum mechanics framework for inducing orientation, typical magnetic field orientation setups, and a summary of latest advances in their use to enhance the performance of materials. Current trends, limitations of current alignment techniques are highlighted and major challenges in the field are identified.

1. Introduction

Graphene is an allotrope of Carbon that exist as a planar sheet consisting of carbon atoms arranged in a hexagonal lattice, much like a honeycomb structure [1,2]. Each carbon atom exhibits sp^2 hybridization, where it is bonded to 3 other carbon atoms through the plane π bond and in-plane σ bonds with conjugate π-π bonding throughout the surface. This special arrangement of C atoms endows extraordinary chemical and physical properties to a graphene monolayer [3]. While multilayer graphene is formed by stacking various monolayers one above another, the material is termed graphite as the number of layers exceeds a certain limit (usually more than 10 layers) [4]. Graphene as graphite has existed in the scientific literature for a long time; its practical exfoliation, including sulfuric acid (H_2SO_4) and nitric acid (HNO_3) to obtain graphene oxide dates back almost 170 years [5,6]. Later, in 1859, Brodie, a British scientist, revised the synthetic mechanism by adding $KClO_3$ as an oxidant to the process [7]. The lamellar stacking of graphene is the result of the chemical oxidation process of GO surface reducing the forces occurring in the inter-planar surfaces. Further, Offman and Hummer, in 1858, brought up a novel mechanism for graphite oxidation using H_2SO_4 and potassium permanganate [8]. Extensive graphene research has been ongoing since then, while in 1947, the electronic structure of graphene was established by P.R. Wallace [9]. Subsequently, a number of modifications and mechanisms have been studied by various researchers to isolate single layers of graphene from bulk graphite and derived materials. Graphene emerged as a wonder material as single layers of graphene were isolated following a mechanical exfoliation process called the scotch tape method by Novoselov and Geim in 2004 [1–3]. The extraction of thin layers took the researchers and material scientists' world by storm. Thereafter, graphene attracted much interest and revolutionized the field of low-dimensional materials. Graphene exhibits extraordinary properties such as a large surface area, excellent mechanical strength,

* Corresponding authors.
E-mail addresses: ghai@chalmers.se (V. Ghai), roland.kadar@chalmers.se (R. Kádár).
[1] Authors with equal contribution.

https://doi.org/10.1016/j.pmatsci.2024.101251
Received 8 August 2023; Received in revised form 31 October 2023; Accepted 6 February 2024
Available online 11 February 2024

Nomenclature

BMI	Bismaleimide
CIPs	Carbonyl iron particles
CMF	Constant magnetic field
CNTs	Carbon nanotube
DMF	N, N-dimethyl formamide
EMI	Electromagnetic interference
E. coli	*Escherichia coli*
FPAPB	Fluorinated poly arylene propane biphenyl
G	graphene
GNPs	Graphene nanoplatelets
GO	Graphene oxide
HEMA	2-hydroxyethyl methacrylate
M_r	Saturation remanent magnetization
PAMPS	Poly(2-acrylamide-2-methyl-1-propane sulfonic acid)
PDMS	Polydimethylsiloxane
PVA	Polyvinyl alcohol
PVD	Physical vapor deposition
PVDF	Polyvinylidene fluoride
rGO	Reduced graphene oxide
SEM	Scanning electron microscopy
SPEEK	Sulfonated polyether ether ketone
G_S	Sulfonated graphene
XRD	X-ray diffraction
WPU	Waterborne polyurethane

and high electrical and thermal conductivity [10]. Since graphene has a planar geometry, the highly exposed surface area through both sides of the monolayer can serve as an active site for a number of chemical reactions and physical phenomena such as adsorption, heterogeneous catalysis, etc. [11,12]. As determined by atomic force microscopy, free-standing graphene has an excellent mechanical (tensile) strength of 42 Nm^{-1} with 1 TPa Young's Modulus, thus making it the toughest known material [13]. High mechanical strength is attributed to the covalent σ bonds resulting in a short interatomic distance of ~1.42 Å, shorter than the diamond's sp^3 hybridized C–C bond length. Graphene is a semiconducting material possessing zero band gap, where electrons and holes act as charge carriers. The bonding (valence band) and anti-bonding (conduction band) π-orbitals present above and below the hexagonal plane dictate the electronic conductivity. The exceptional electronic conductivity and intrinsic charge carrier mobility endow graphene with excellent potential in electronic devices and applications [10]. Being the strongest and lightest material having extraordinary characteristic properties, graphene gained much publicity/popularity. It emerged as a versatile material, finding applications in numerous/innumerable disciplines such as energy technology, bioengineering, optoelectronics, spintronics, nanotechnology and many more [10–12]. Graphene is believed to be the future of bioengineering, where various reports suggest its usage in sensing devices for monitoring cholesterol, glucose, hemoglobin, etc. Moreover, the biocompatibility and biotoxicity of graphene and its potential uses in tissue regeneration have been realized [14]. As LCD (liquid crystal display), OLEDs (organic light emitting diode), and touchscreens continue to dominate commercial technology, the field of optoelectronics relies on highly optically transparent and electrically conductive material as the future [15]. Graphene's ability to transmit 97.7 % light, in addition to its high tensile strength, adds to its efficiency as an effective material in advanced technologies like portable computers, desktops, mobile phones, tablets, etc. [16].

Although graphene exhibits excellent characteristics, the practical realization of the applications on a large scale is hindered in many cases because of the anisotropic nature of its intrinsic physical and chemical properties. Therefore, to replicate the outstanding merits of graphene on an industrial scale, graphene is added as a filler to polymers, ceramics and metals to achieve highly flexible, strong and conductive composite materials. As a filler, graphene not only enhances the efficiency of existing technologies but also creates a novel class of materials with superior qualities, enhanced performance and a diverse range of applications. Owing to their light weight, flexibility, strength, and electrical and thermal conductivity, graphene composites find potential in aerospace materials, medical implants, weatherproofing and many more. The tailoring of material properties according to the application of the graphene composite majorly depends on the (a) amount of graphene added as filler to the matrix, (b) orientation and distribution of different layers of graphene and (c) the graphene and matrix interface. It should be noted here that while interface regulation is a fundamental step in creating graphene composites (good adhesion and dispersion), it may not fully optimize the material for all desired applications. The advantages of controlling orientation come into play when the specific properties and characteristics of the composite need to be fine-tuned to meet the requirements of diverse applications, including those where anisotropic or highly directional properties are needed. Therefore, the effective transfer of microscopic properties of graphene to real-life macroscopic applications relies on the control and management of the alignment of the planes of each unit of the graphene sheet.

Three main methods to achieve a specific orientation of graphene based on field-filler interaction have been put forth in the

literature: flow-induced orientation, electric field-induced orientation and magnetic field-induced orientation. In flow-induced orientation, shear and extensional flows are used to orient the nanofillers mainly in the flow direction [17–19]. The most used processes, applicable to thermoplastic polymers, are extrusion and injection molding, demonstrating the orientation of both isotropic and anisotropic nanoparticles such as GNPs, CNTs, TiO_2 and graphene [20–24]. However, flow-induced orientation has several limitations, such as the high viscosity of the filled polymers, and alignment gradients due to shear and extensional rate gradients in flow [18]. Therefore, achieving a uniformly distributed oriented nanofiller in a polymeric matrix is challenging. Furthermore, orientation in the flow direction can also be a limiting factor in terms of applications. Highly oriented composites can be fabricated using an electric field. To align graphene nanosheets, direct or alternating current can be used. However, with direct current, the negatively charged graphene sheets underwent electrophoretic migration toward the cathode, leading to electrochemical reduction of the cathode [25]. When an alternating current is supplied, the dipole moment, which is not aligned earlier, tends to align in the direction of the field applied [26,27]. Despite getting aligned graphene sheets in composite, the applied electric field has several limitations, such as a need for ultra-high voltage due to the high viscosities usually involved, bulky setup, the influence of pH and electric charge on particles, due to the breakdown voltage of polymer and production of only small-scale aligned films [18,26,28]. Due to these limitations for both flow and electric fields, magnetic field-assisted alignment has emerged as the most attractive and easy-to-manipulate filler alignment in the desired directions. Moreover, the magnetic field could provide a uniform, flexible, contactless and scalable approach to aligning graphene nanosheets; see the overview Fig. 1 [18].

It should be noted that aligned graphene sheets can also be fabricated using chemical vapor deposition; however, it is not part of this review. It would be essential here to highlight that there have been several reviews on strategies to align nanomaterials in the polymer [17–19,26,29–32]. However, there is no review describing the current status of graphene orientation under a magnetic field. Therefore, this review will focus solely on the alignment of graphene and its derivatives in magnetic fields.

The manuscript is organized as follows. In section 2, general considerations on the magnetization of materials are presented,

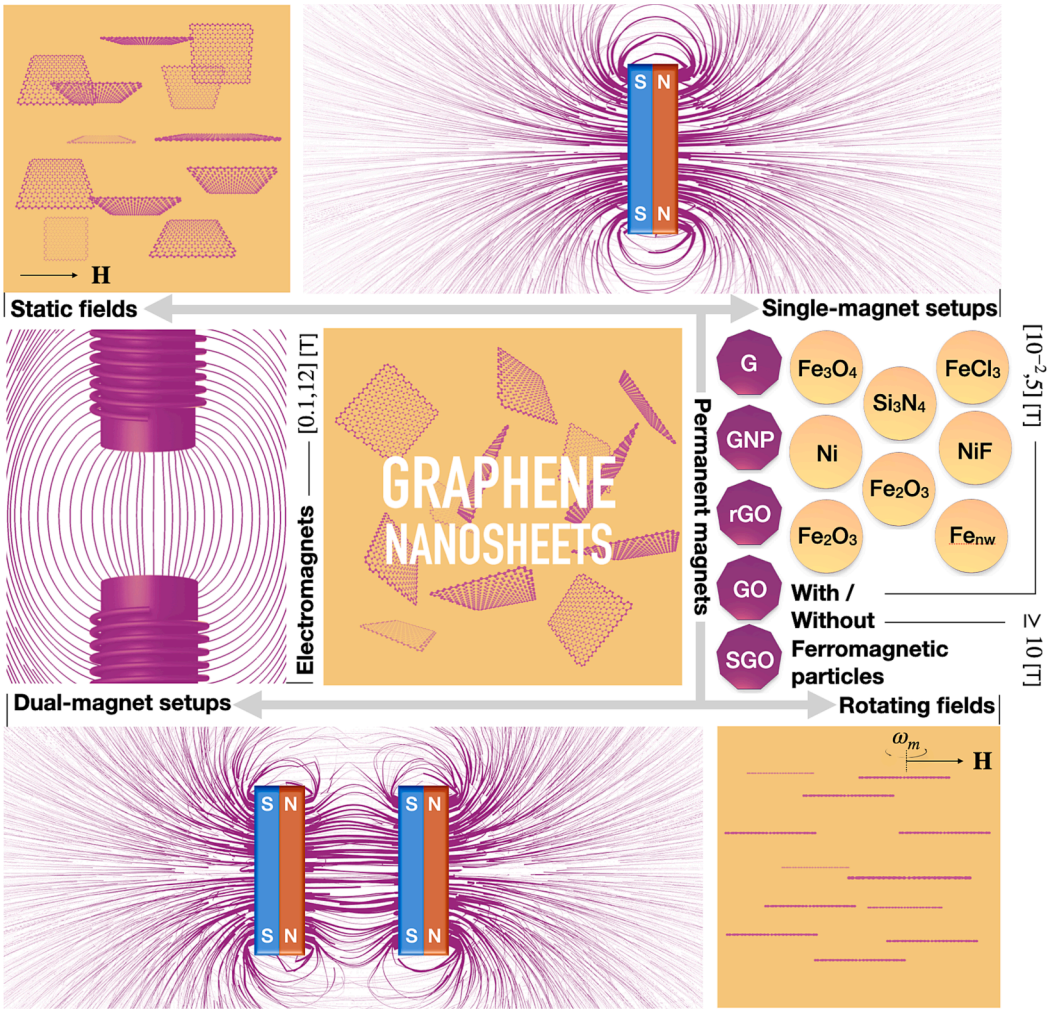

Fig. 1. Overview figure outlining the main aspects of magnetic field induced orientation of graphene nanosheets.

followed by how specific mechanisms thereof in graphene. Section 3 includes a general theoretical magneto-hydrodynamic framework for the orientation of graphene using magnetic fields in quiescent fluids and a general overview of the experimental setups used therefore. In section 4, we review the available scientific literature on the orientation of graphene in magnetic fields followed by section 5 where current trends, limitations and challenges with future prospects are provided.

2. Magnetization in materials

Two major factors providing magnetization in any material are the orbital movement of electrons and the spin of electrons, as shown in Fig. 2. The first is due to the movement of unpaired electrons in orbit, which causes an electric charge in motion. The moving electric charge produces an electromotive force leading to a magnetic dipole moment. The second factor which provides magnetism is the spin motion of each electron. Therefore, the overall net magnetic moment in an atom is the vector sum of its orbital and spin magnetic moments. Based on their magnetism, materials have been broadly categorized as ferromagnetic, paramagnetic, diamagnetic, and antiferromagnetic.

Ferromagnetism and Antiferromagnetism

The most common ferromagnetic materials known are iron (Fe), cobalt (Co) and nickel (Ni). The electronic configuration of these materials has 4, 3 and 2 unpaired electrons, respectively. Due to the combination of both non-cancelable electronic spin and the presence of these unpaired electrons, Fe, Co and Ni show permanent magnetic moments without the application of an external magnetic field, phenomenon known as spontaneous magnetization (Fig. 3a). This spontaneous magnetization is generated in several domains of ferromagnetic materials leading to the highest magnetic susceptibility. However, in the absence of an external field, the magnetization vector of these domains is randomly arranged and therefore has zero net magnetization. That is why these materials do not behave like a magnet at room temperature without any external field. When an external magnetic field is applied, these randomly arranged domains are reoriented towards the magnetic field direction (Fig. 3a). It should be noted that spontaneous magnetization is only achievable below the Curie temperature of the material. Above the Curie temperature, ferromagnetic materials behave similarly to paramagnetic materials. In contrast, antiferromagnetic (Fig. 3b) materials (and ferrimagnetic) have magnetic dipoles aligned in opposite directions, thereby reducing the magnetic susceptibility of the material (Fig. 3b). One of the significant applications of these materials is in reading and writing information on electronic devices such as hard disks.

Paramagnetism

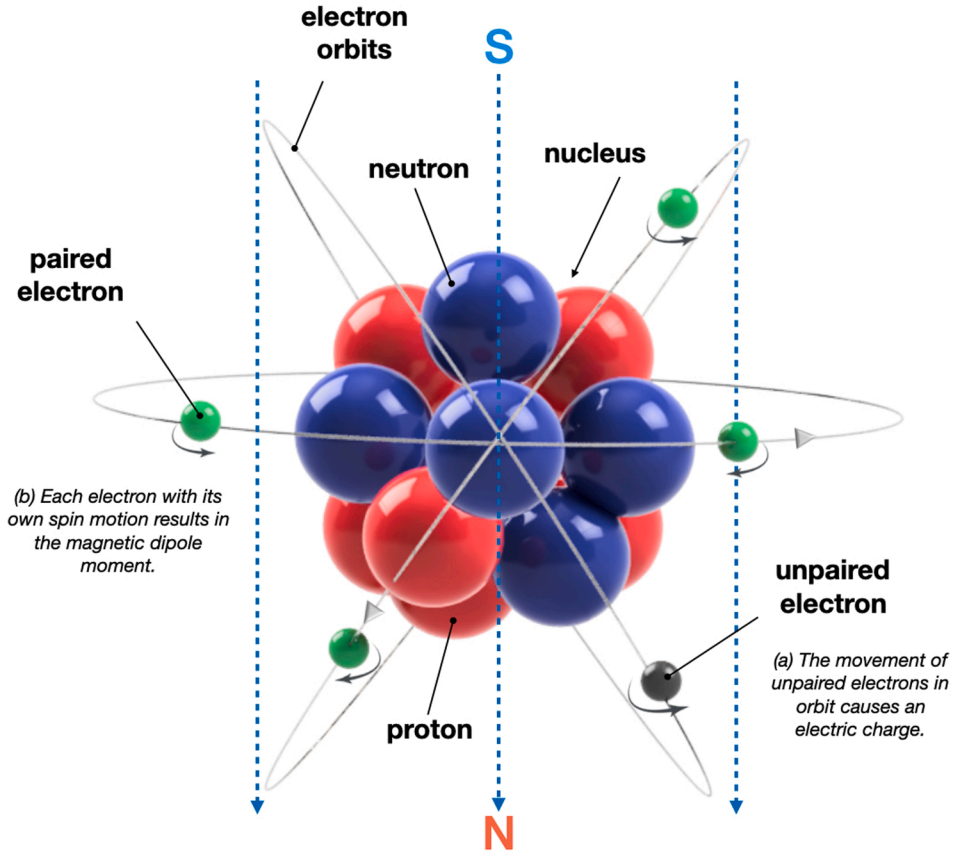

Fig. 2. Illustration showing the presence of magnetic moments due to the orbital moment of electrons and intrinsic spin moments of electrons.

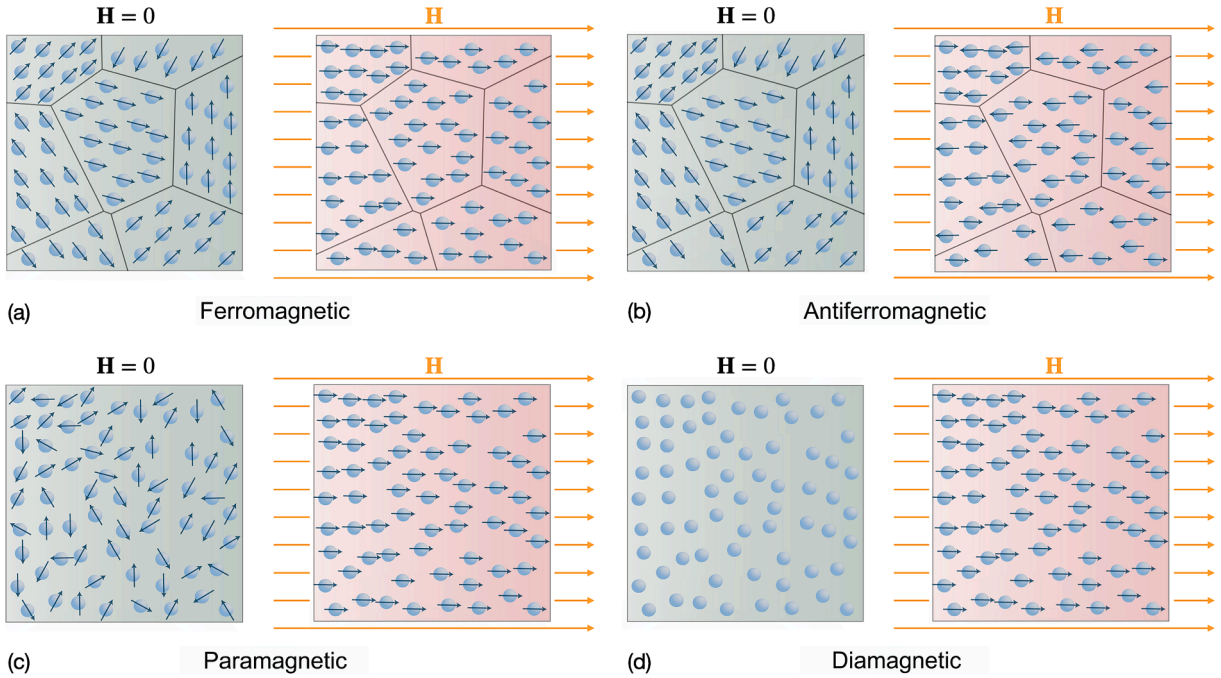

Fig. 3. Magnetic dipole moment in materials with and without applied external magnetic field (a) ferromagnetic, (b) antiferromagnetic, (c) paramagnetic, and (d) diamagnetic.

Paramagnetic materials show far less magnetic susceptibility than ferromagnetic materials and therefore, an external magnetic field is always required to observe magnetization. Due to unpaired electrons in partially filled orbitals, the magnetic moment in paramagnetic materials is also observed without an external magnetic field. However, similar to ferromagnetic materials paramagnetic materials also require an external magnetic field to align all the domains (Fig. 3c). One special case of paramagnetism is super-paramagnetic materials; these are ferromagnetic materials with an extremely small size (5 to 30 nm), and their magnetization direction highly depends upon the temperature. These nanoparticles are mostly stable in aqueous solutions and find several potential applications as ferrofluids.

Diamagnetism

Diamagnetic materials have low magnetization due to filled orbitals. These materials have no free electrons; therefore, there is no magnetic moment without an external magnetic field. Moreover, the generated magnetic moment due to the orbital motion of electrons is opposite to an applied magnetic field (Fig. 3d). Therefore, diamagnetic materials show a negative susceptibility, as the produced magnetic moment repels the material from magnetic fields.

2.1. Fundamental magnetization mechanisms in pristine graphene.

Pristine graphene, a diamagnetic material, exhibits a characteristic response that opposes the applied field when placed in an external magnetic field. This behavior arises from Lenz's law, which states that a changing magnetic field induces a current that creates a magnetic field opposing the change [33]. Pristine graphene has no intrinsic magnetic moment or net magnetization in the absence of an external field [34]. However, when subjected to a magnetic field, the external field induces a weak magnetic moment in pristine graphene nanosheets that aligns itself opposite to the applied field. The induced magnetic moment in graphene is a consequence of the orbital motion of its π-electrons. In a magnetic field, these π-electrons experience a Lorentz force that causes their orbits to adjust [33]. As a result, the electron cloud of graphene undergoes a subtle redistribution, leading to the generation of a weak magnetic moment that opposes the external magnetic field. As a result, a repulsive force is experienced between the pristine graphene and the external field [35]. This repulsion causes the material to orient itself in a way that minimizes its interaction with the external field. However, it's important to note that this effect of diamagnetism in pristine graphene is relatively weak due to several factors. Firstly, graphene has a low electron density, resulting in a reduced number of charge carriers available for orbital rearrangement. Additionally, the intrinsic properties of graphene, such as its unique electronic structure, contribute to the small induced magnetic moment. The magnitude of the induced magnetic moment in graphene is typically on the order of 10^{-6} to 10^{-8} Bohr magnetons per carbon atom, where a Bohr magneton is a unit of the magnetic moment [34]. This value is several orders of magnitude smaller than the magnetic moments observed in paramagnetic or ferromagnetic materials. Therefore, to orient pristine graphene nanosheets, ultra-high magnetic fields of 10–12 T are required [36]. Additionally, the weak induced magnetization in pristine graphene decreases as the temperature increases. Due to these weak effects, the orientation of diamagnetic pristine graphene nanosheets in a magnetic field is not readily visually perceptible. However, sensitive measurement techniques can detect the subtle changes in magnetization and magnetic susceptibility of

diamagnetic materials when subjected to a magnetic field [37,38].

2.2. The role of defects in the magnetization of graphene

Graphene being a 2D aromatic material, its susceptibility is extremely anisotropic, i.e., tailoring the band structure of graphene by introducing different types of defects or doping graphene nanosheets could change the local electron state due to delocalized π electrons and localized spin could lead to developing a magnetic moment [39–45]. Magnetic moment in graphene could be introduced through various methods. One common approach is introducing defects; these defects can be introduced either by slicing/cutting the graphene sheets into nanoribbons or by creating vacancies in the graphene sheets. The graphene nanoribbons are broadly classified as armchair nanoribbons and zig-zag nanoribbons. The zig-zag configuration has unpaired electrons at its edges along with localized spins. These free electrons and localized spins impart magnetism in the graphene sheets [46]. The infinite or pristine graphene sheet has zero dipole moments or magnetism because there are no free electrons and only delocalized π electrons in conjunction with each other. But when we slice the graphene sheets the effect of the edge becomes significant because by slicing the edge, π bonds are now the free electrons. In graphene nanoribbons, the Lorentz force drives delocalized π electrons to move in the graphene (basal plane due to its 2D structure; see also Fig. 4a) sheets, inducing ring current in aromatic rings and an anisotropic magnetic field [35,47]. This anisotropic magnetic field is due to an anisotropic 2D structure. This further imparts a different magnetic susceptibility along the graphene in-plane (basal plane or conjugated plane or *c*-axis or easy axis) and out-plane (edge plane or *a*-axis or hard axis) directions (Fig. 4a). Experimentally it is found that even the sliced graphene nanosheets with zig-zag edges have much higher diamagnetic susceptibility in the *c*-axis compared to the *a*-axis. Thus, given a static magnetic field of sufficient strength, graphene nanosheets will orient with the *c*-axis perpendicular to the magnetic field lines, Fig. 4a. Consequently, the *a*-axis can have any angular position with respect to the *c*-axis and graphene nanosheets and the basal plane could have any angular position around the *a*-axis. In contrast, in a rotating magnetic field of sufficient strength and angular frequency, ω_m, the *c*-axis is perpendicular to the plane of rotation of the magnetic field and thus the basal plane loses its degree of freedom around the *a*-axis, Fig. 4b. This is further discussed in the following sections.

The overall magnetic susceptibility of sliced graphene is very low compared to several paramagnetic and ferromagnetic materials but higher than the pristine graphene nanosheets. Experimental introduction of defects in graphene through slicing or cutting and subsequently controlling the magnetization of the sliced graphene poses significant challenges.

Nevertheless, one of the commonly employed methods for synthesizing graphene with defects is through a chemical route, known as Hummer's method, which results in graphene oxide (GO). It is important to note, however, that this method introduces oxidation defects in GO and leads to the presence of various functional groups on rGO. Despite these defects, GO and rGO do not exhibit magnetic properties to the extent desired for orientation applications.

To address the limitation of oxidation defects, additional defects can be introduced, such as the adsorption of ferromagnetic or superparamagnetic particles, in order to impart magnetic properties to the nanofillers. In this method, superparamagnetic/ferromagnetic materials are adsorbed on the graphene nanosheets to modify the density of π-states [43]. These nanoparticles, when attached to graphene, not only allow graphene to retain its properties but also add other advantages, such as superparamagnetism, low toxicity, high catalytic activity, and biocompatibility with the environment [43,48]. These superparamagnetic nanoparticles have free dipole moments; therefore, when attached to graphene, they align the graphene's basal plane parallel to the direction of the applied

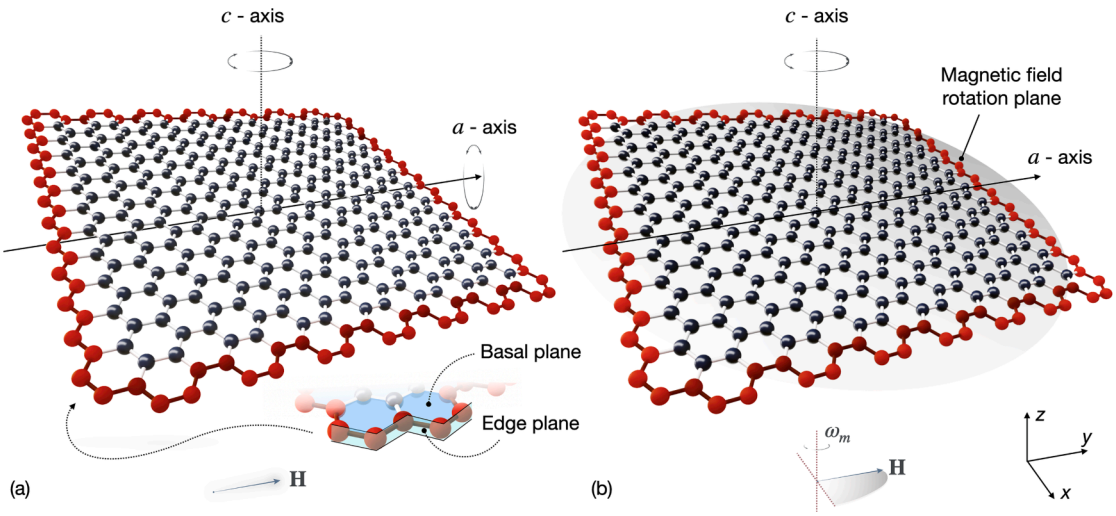

Fig. 4. Schematic of graphene nanosheets and orientational configurations in (a) static magnetic fields where the *c*-axis is perpendicular to the direction of magnetic field and thus nanosheets have orientational degrees of freedom as rotation around the *c*-axis as well as around the direction of the applied magnetic field and (b) rotational magnetic fields where the *c*-axis is perpendicular to the plane of rotation of the applied magnetic field, thus allowing only rotation around the *c*-axis. We note that the rotation around the *c*-axis will not influence the anisotropic properties of a composite.

magnetic field, Fig. 4 [49]. With the attachment of magnetic particles strong magnetization can be achieved due to their interaction with each other. Semiconducting π electrons from graphene sheets and magnetic d electrons from superparamagnetic particles interact through d-π electron coupling based on long-range coulomb interactions and short-range spin–spin interactions [50]. Under an external magnetic field, both Coulomb interaction and spin–spin interaction between d electron in magnetic nanoparticles and delocalized π electron in graphene can be enhanced and lead to the alignment of graphene sheets at relatively low magnetic fields (9–50 mT) [50–53].

There have been several methods reported for synthesizing G@ferro/superparamagnetic nanohybrids, as shown in Table 1. The most common ferromagnetic particles used to fabricate magnetic graphene are iron; nickel and cobalt exhibit genotoxicity and carcinogenicity and are, therefore, unsuitable for several bio-related applications [54]. Magnetic graphene can be fabricated by hydrolysis, co-precipitation, solution processing, hydrothermal, solvothermal, mechanical mixing, or by adsorption of nanoparticles.

Another method to introduce magnetic properties in graphene involves functionalizing graphene with organic molecules such as Nitrophenyl or hydroxyl group [34,85]. By attaching such molecules to the graphene surface, magnetic interactions can be introduced, resulting in magnetism. It is worth noting that while magnetism can be induced in graphene through these methods, the resulting magnetic properties are generally weaker compared to conventional ferromagnetic materials. However, a few studies have also shown that graphene nanosheets could behave as paramagnetic with modification in the synthesis process. This way, alignment could be obtained with a magnetic field of as low as 24 mT [86]. Additionally, the precise nature and strength of magnetism in graphene depend on the specific method of induction and the surrounding environment. Moreover, several researchers have already reported details of magnetism in graphene nanosheets. Therefore, we direct readers toward these reviews for an in-depth study of magnetism in graphene nanosheets [87–91].

To summarize, two major methods are commonly used to make it possible for graphene nanosheets to orient using magnetic fields in various matrices or solvents. In the first method, graphene is decorated with one type of paramagnetic/superparamagnetic nanoparticle (Fe, Co, Ni). Graphene alignment is obtained by placing it in a magnetic field. In the second method, the low diamagnetic nature of graphene due to defects can be exploited for orientation using ultra-high magnetic fields (more than 9 T).

3. Techniques to align graphene nanosheets in magnetic field

Graphene doped with or without ferromagnetic particles can be aligned in the magnetic field broadly in two ways, i.e., using a permanent magnet system (single magnet system and dual magnet system) or an electromagnet. Here, it is very important to define alignment order before we discuss the alignment in graphene-based composites. Alignment order is the degree and organization of graphene sheets within a composite when they are aligned using any external field/force. In the current work, “alignment order” would describe how well the graphene sheets are aligned in the composite material under the influence of a magnetic field. It can range from a highly ordered structure, where the graphene sheets are perfectly aligned in the direction of the magnetic field, to a more disordered or random arrangement. The alignment order in such materials is crucial because it can significantly influence their electrical, mechanical, and thermal properties. Further, to achieve a higher alignment order, these systems (single and dual magnet systems) are divided to provide static or rotational magnetic fields.

3.1. Theoretical background

The theoretical framework below is written with an emphasis on the hydrodynamic part, whereas more detailed elaborations emphasizing the magnetic fields can be found in the works of Erb et al., (2012) and Wu et al., (2016) [51,52,92]. The goal of this subsection is to provide a general overview on estimations of the torques and orientation times associated with the motion of an arbitrary-shaped nanoparticle bound by a surface $\mathscr{A}$ in a quiescent infinite purely viscous incompressible fluid under the action of an arbitrary external field, ignoring any gravitational effects, is described by the well-known Navier-Stokes and continuity equations [93,94].

$$\rho \frac{D\mathbf{v}}{Dt} = \nabla \cdot \mathbf{S} + \mathbf{f}_b \tag{1}$$

$$\mathrm{tr}\mathbf{D} = 0 \tag{2}$$

Table 1
Various techniques for the synthesis of magnetic graphene nanosheets.

Elements	Graphene oxide (GO)	Reduced graphene Oxide (rGO)	Graphene nanoplatelets (GNPs)	Graphene (G)
Fe	Hydrolysis process[43], Hydrothermal method[55–57], Solution process[58–64], Molecular-level-mixing[65], Solvothermal method[66], co-precipitation[67–72]	Adsorption[73,74], Solvothermal method [48]	Mechanical Mixing[75,76], Adsorption[77–79], co-precipitation [52,80], Solvothermal method[28]	
Co				CVD Method[81], One step laser scribing[82]
Ni	Molecular-level-mixing[83], Solution process[49]		Mechanical Mixing[84]	

where ρ is the density, $D\bullet/Dt = \partial\bullet/\partial t + \mathbf{v}\cdot(\nabla\bullet)$ is the material derivative of the velocity vector $\boldsymbol{v}$, η_0 the shear viscosity, $\nabla = \mathbf{e}_1\partial/\partial x_1 + \mathbf{e}_2\partial/\partial x_2 + \mathbf{e}_3\partial/\partial x_3$ is the del (or nabla) differential operator, $\mathbf{S}$ is the total or Cauchy stress tensor, $\mathbf{f}_b$ are general body forces, and $\mathbf{D}$ is the rate of deformation tensor. In the case of a pure viscous (Newtonian) fluid, the stress tensor can be expressed as $\mathbf{S} = -p\mathbf{I} + 2\eta_0\mathbf{D}$, where p is the isotropic pressure and $\mathbf{I}$ the unit stress tensor. Further assuming that the Reynolds number of the particle, $Re_p = \rho_p v_p d_p/\eta_0$, is small $Re_p \ll 1$, where ρ_p is the density of the particle, v_p is a characteristic particle velocity and d_p is a characteristic lengthscale of the nanoparticle, and that far from the nanoparticle the fluid is undisturbed by the motion of the particle Equation (1) reduces to the Stokes approximation:

$$0 = -\nabla p + \eta_0\nabla^2\mathbf{v} \tag{3}$$

where any other effects (body forces) are neglected. Considering the nanoparticle is rigid and O is its geometric center, the motion of the particle is therefore described by a translational velocity in the center of the particle $\mathbf{v}_0$, and a rotation with angular velocity ω as:

$$\mathbf{v}_p(\mathbf{x}) = \mathbf{v}_O + \omega \times \boldsymbol{x} \tag{4}$$

where $\mathbf{x}$ is the coordinate vector from the center of the particle. The resultant forces and stresses generated by the motion of the particle under the influence of an external field in a Stokes flow, and using the associated Lorentz reciprocal relations [94], i.e., $\mathbf{f} = \int_{\mathscr{A}}\mathbf{S}\cdot\mathbf{n}d\mathscr{A}$ and $\mathbf{g} = \int_{\mathscr{A}}\mathbf{x}\times(\mathbf{S}\cdot\mathbf{n})d\mathscr{A}$, can therefore be expressed as [93,94]:

$$\mathbf{f} = -\eta_0\left(a\mathbf{A}_1\cdot\boldsymbol{v}_p + a^2\mathbf{A}_2\cdot\omega\right) \tag{5}$$

$$\mathbf{g} = -\eta_0\left(a^2\mathbf{A}_3\cdot\boldsymbol{v}_p + a^3\mathbf{A}_4\cdot\omega\right) \tag{6}$$

where $\mathbf{A_1}$, $\mathbf{A_2}$, $\mathbf{A_3}$, $\mathbf{A_4}$ are called resistance tensors and are uniquely determined for a particular particle shape. The minus sign in Equations. (5)-(6) signifies the resistance to flow under the action of the external field. Consequently, the translational and rotational components of the particle motion under the influence of the external field can be determined as [93,95]:

$$\mathbf{v}_0 = \frac{1}{\eta_0 a^2}\left(a\mathbf{A}_1^{'}\cdot\mathbf{f}_{\boldsymbol{m}} + a\mathbf{A}_2^{'}\cdot\mathbf{g}_{\boldsymbol{m}}\right) \tag{7}$$

$$\omega = \frac{1}{\eta_0 a^3}\left(a\mathbf{A}_3^{'}\cdot\mathbf{f}_{\boldsymbol{m}} + a\mathbf{A}_4^{'}\cdot\mathbf{g}_{\boldsymbol{m}}\right). \tag{8}$$

where $\mathbf{A}_1^{'}$, $\mathbf{A}_2^{'}, \mathbf{A}_3^{'}, \mathbf{A}_4^{'}$ are the analogous mobility tensors. We note that Equations. (5)-(8) are valid for any external field such as gravitational, electric, or magnetic. However, the notations for force and torque introduced in equations (7)-(8), $\mathbf{f}_{\boldsymbol{m}}$ and $\mathbf{g}_{\boldsymbol{m}}$ refer to specifically the magnetic counterparts. Explicit relationships between the resistance and the mobility tensors can be found elsewhere [96]. While the present review concerns 2D nanoparticles (graphene), we note that all particles with fore-aft symmetries, such as prolate and oblate spheroids, have qualitatively identical governing equations and dynamics [94,96].

The propagation of electromagnetic waves in condensed matter media is governed by Maxwell's equations [33]:

$$\nabla\cdot\mathbf{D} = \rho_e \tag{9}$$

$$\nabla\times\mathbf{H} - \frac{\partial\boldsymbol{D}}{\partial\boldsymbol{t}} = \boldsymbol{J} \tag{10}$$

$$\nabla\times\mathbf{E} + \frac{\partial\boldsymbol{B}}{\partial\boldsymbol{t}} = 0 \tag{11}$$

$$\nabla\cdot\mathbf{B} = 0 \tag{12}$$

where $\mathbf{E}$ and $\mathbf{B}$ are the electric and magnetic induction fields, $\mathbf{D}$ and $\mathbf{H}$ are the electric displacement and magnetic fields, and $\rho_e(\mathbf{x})$ and $J(\mathbf{x})$ are the charge and current densities in the media, respectively. We briefly note that while in the formulation of the Navier-Stokes equations it is rather common to strictly distinguish between vectors (lowercase bold letters) and tensors (uppercase bold letters) this convention does not typically extend to Maxwell's equations. For magnetostatic fields, Equations. (9)-(10) for the magnetic field become [33]:

$$\nabla\times\mathbf{H} = \boldsymbol{J} \tag{13}$$

$$\nabla\cdot\mathbf{B} = 0 \tag{14}$$

In the presence of magnetizable media, the relationship between $\mathbf{B}$ and $\mathbf{H}$ is:

$$\mathbf{B} = \mu_0(\mathbf{M} + \mathbf{H}) \tag{15}$$

where μ_0 is the permeability of vacuum and the magnetization $\mathbf{M}$ is the average magnetic moment density in the magnetic media, i.e.,

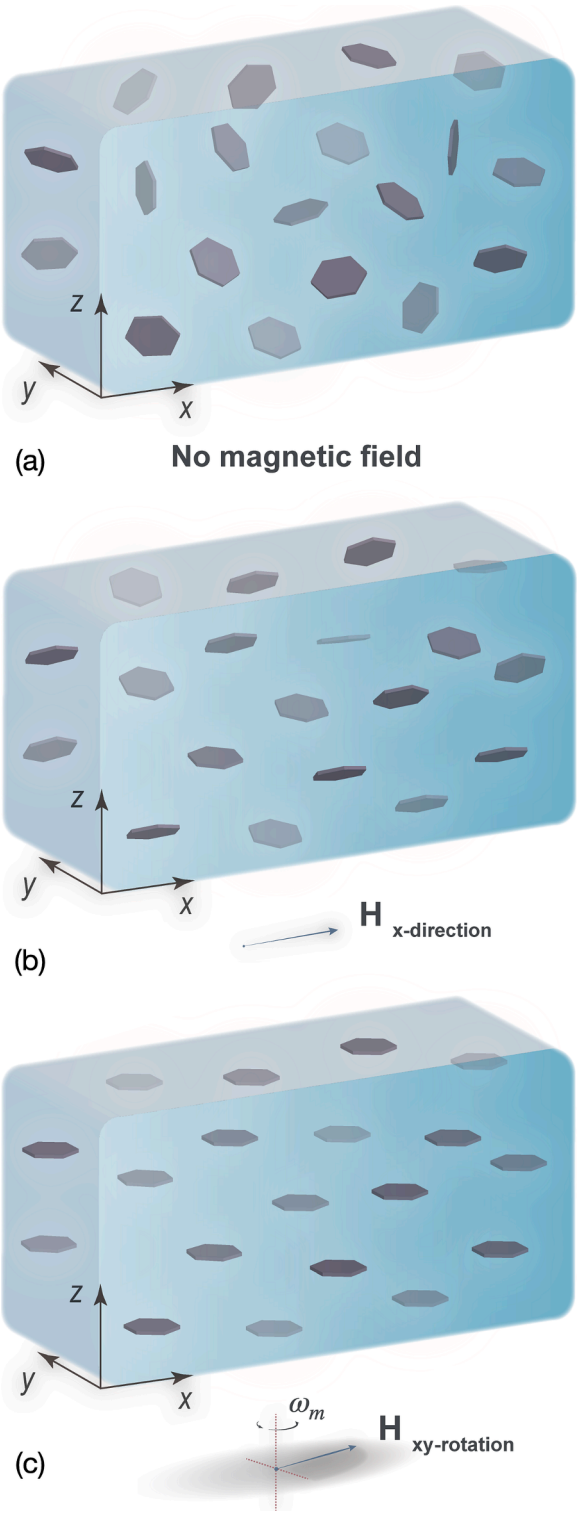

Fig. 5. Schematic showing (a) random orientation in the absence of a magnetic field, (b) orientation induced by a static and (c) rotating magnetic field.

$\mathbf{m} = \int_{\mathscr{V}} \mathbf{M}(\mathbf{x}) d\mathscr{V}$, with $\mathbf{m}$ being the total magnetic moment and $\mathscr{V}$ the volume of the magnetic media. As already mentioned, when subjected to an external magnetic field, graphene sheets impart a magnetic field opposite to the applied field [35]. Due to this, a magnetic dipole is created, and the magnetic dipole further creates a torque to rotate the graphene sheets with their hard plane parallel to the applied field, see Fig. 4. For 2D nanosheets having magnetic nanoparticles attached or are intrinsically magnetic due to the presence of surface defects, the magnetic force and torque exerted by the applied magnetic field can thus be approximated as:

$$\mathbf{f}_m = \nabla(\mathbf{m} \cdot \mathbf{B}) \tag{16}$$

$$\mathbf{g}_m = \mathbf{m} \times \mathbf{B} \tag{17}$$

Thus, using Equations (5)-(6) and (16)-(17) the equations of motion for the motion of a 2D nanoparticle in magnetic field become

$$\mathbf{f} + \mathbf{f}_m = 0 \tag{18}$$

$$\mathbf{g} + \mathbf{g}_m = 0 \tag{19}$$

Substituting Equations. (16)-(17) into (7)-(8) allows for the exact determination of the particle motion. General procedures for solving the equations of motion (Equations. (18)-(19)) are from hydrodynamic point of view essentially extensions of spheroidal particles. The force $\mathbf{f}$ for a translating rigid sphere of diameter $2a$ resulting from Equation (5) is the well-known Stokes' Law, $\mathbf{f} = \zeta v_0$, where $\zeta = 6\pi\eta a$ is sometimes called the friction coefficient for the particle [94]. Similarly, considering Stokes' law for a rotating sphere the hydrodynamic torque, resulting from Equation (6) can be expressed as $\mathbf{g} = \zeta_r \omega$ where $\zeta_r = 8\pi\eta a^3$ is the rotational friction coefficient. Based on this, the rotational friction coefficient of non-spherical particles can be approximated as

$$T_v = 6\eta V \frac{d\varphi_p}{dt}\left(\frac{k}{k_0}\right) \tag{20}$$

where V is the volume of the arbitrary particle, with $V = 2\pi ab^2$ for oblate ellipsoids, $\omega = d\varphi_p/dt$ is the particle rotation, and the correction factor (k/k_0) quantifies the deviation of the ellipsoid from a sphere, also known as the Perrin factor [51,97]. The particle rotation in equation (20) was expressed as the time derivative of the angle φ_p with respect to an arbitrary absolute coordinate system as means to determine the timescales associated with orientation in magnetic fields.

We note that the equations of motion (18)-(19) exclude other body forces such as gravity, solvent-molecular collision, and solvent-dielectric interactions [45]. However, it must be mentioned that considering a colloidally-stable graphene suspension, Brownian motion leads to a stable equilibrium in which graphene sheets are randomly oriented, see Fig. 5a. This can be included in equation (1) in the form of a fluctuating force density body force [94]. Upon the application of an external magnetic field, the potential energy possessed by graphene nanosheets can be given as [35].

$$U = \mathbf{m} \times \mathbf{B} = \frac{Ae^2}{2\pi\mu_{eff}} B^2 \sin^2\theta \tag{21}$$

where A denotes the basal-plane effective area of the nanosheet, μ_{eff} is the effective mass of the p electron in graphene, and θ is the angle formed between the graphene basal plane and the external magnetic field. When $\theta = 0$, the hard (basal) plane of graphene is aligned with the external magnetic field; at this potential energy reaches its minimum so that nanoplatelets tend to align with the external magnetic field and become stabilized according to the principle of minimum potential energy [35,98]. We note that graphene being a 2D structure, the alignment of the hard plane in the direction of the magnetic field leaves the azimuthal angle between the magnetic field and the hard plane arbitrary [99], Fig. 5b Therefore, the basal plane can rotate around the axis of the magnetic field with no alteration of the potential energy of the system [100].

Based on the estimation originally proposed for particles in electric fields [101], an estimation of the magnetic energy for graphene nanosheets approximated as oblate ellipsoids, including the contribution of decorated Fe_3O_4 has been elaborated on by Erb et al.

$$U_m = \frac{2}{3}\pi\left[(b+d)(a+d)^2 - ab^2\right]\mu_f \frac{{\chi_{nh}}^2}{\chi_{nh}+1} H^2 \sin^2\theta \tag{22}$$

In Equation. (22), d is the diameter or thickness of the Fe_3O_4 nanoparticles, respectively, H is the external magnetic field, and the susceptibility being $\chi_{nh} = \frac{\mu_p}{\mu_f} - 1$, where μ_f and μ_p are the magnetic permeabilities of the fluid and the particle. The susceptibility can be approximated as $\chi_{nh} = C_{ff}\chi_{ff}$, where, C_{ff} represents the surface coverage of iron oxide in the shell layer, ranging from 0 to 1, and χ_{ff} represents the susceptibility of the bulk iron oxide [92]. It should be noted that equation (22) is a particular solution for thin platelets $(b/a > 10)$, based on which the geometrical demagnetizing coefficients can be approximated as $G_a \approx 1$ and $G_b \approx 0$ [92]. The magnetic torque T_m required for inducing orientation can now be determined from the magnetic energy as [101].

$$T_m = \frac{dU_m}{d\theta} = \frac{2\pi\mu_f\chi_{nh}^2}{3(\chi_{nh}+1)}\left[(b+d)(a+d)^2 - ab^2\right]H^2 \sin 2\theta \tag{23}$$

Finally, by combining the Equations. (19), (20), and (23), for static magnetic fields $\left(\frac{d\theta}{dt} = -\frac{d\varphi_p}{dt}\right)$ equation

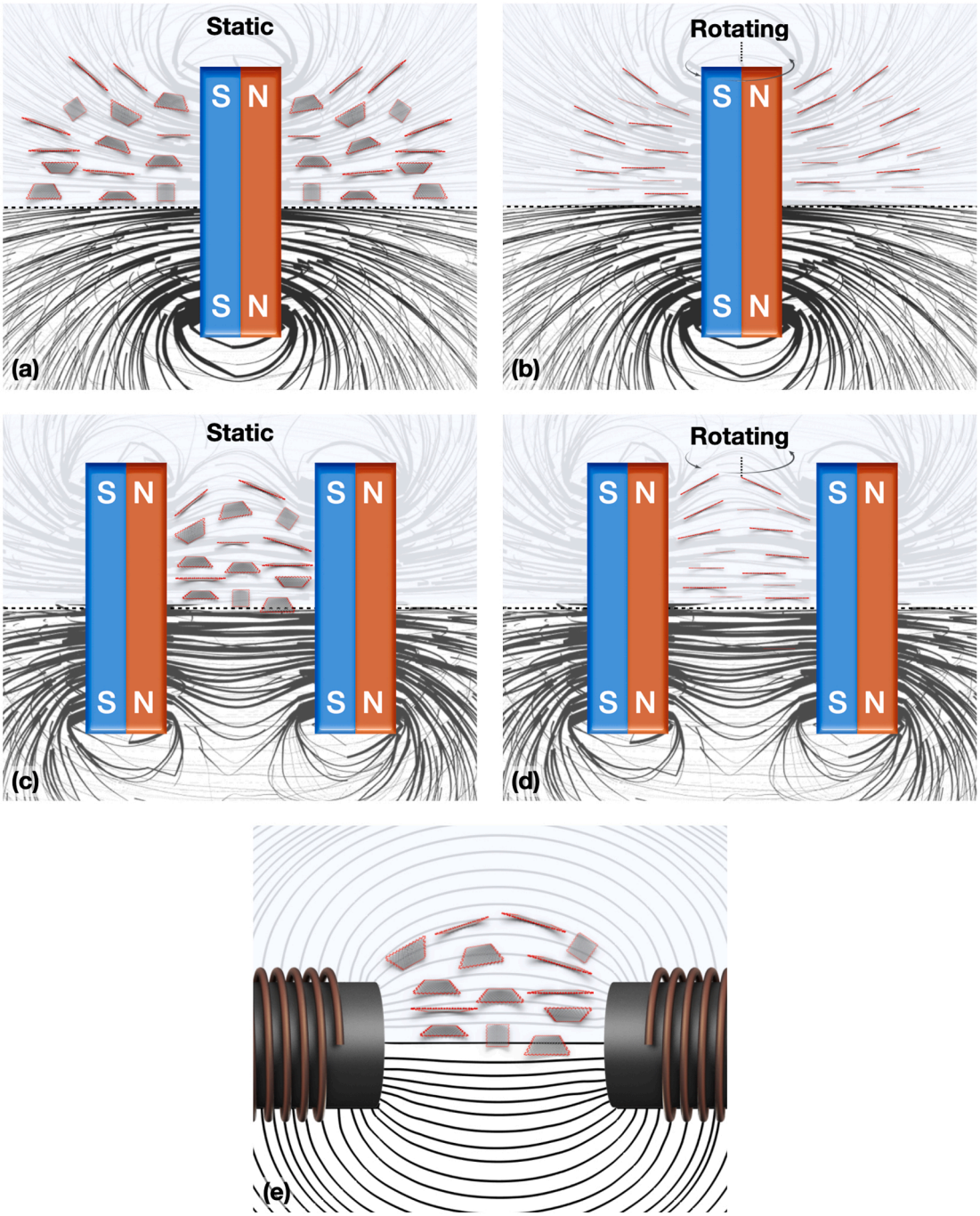

Fig. 6. Different techniques are used to align graphene nanosheets showing magnetic field generated using a single, dual and electromagnet. (a, c, e) representing graphene nanosheets alignment in a static magnetic field in single, dual and electromagnet. Schematic (b and d) represents orientation of graphene nanosheets under a rotating magnetic field in a single and dual magnet configuration.

$$\frac{d\theta}{dt} = -\frac{\mu_f \chi_{nh}^2}{18\eta(\chi_{nh}+1)(\frac{f}{f_0})}\left[\frac{(b+d)(a+d)^2}{ab^2}-1\right]H^2\sin 2\theta \tag{24}$$

can be integrated with respect to time to determine the time required to orient Fe_3O_4/graphene nanosheet from an initial angle θ_1 to a generic angular position θ_2:

$$t_{rot} = \frac{1}{2\omega_c}\ln\frac{\tan\theta_1}{\tan\theta_2} \tag{25}$$

where, $\omega_c = \frac{\mu_f \chi_{nh}^2}{18\eta(\chi_{nh}+1)(\frac{f}{f_0})}\left[\frac{(b+d)(a+d)^2}{ab^2}-1\right]H^2$.

As mentioned in the preceding chapter, applying rotating magnetic fields has the advantage of 'locking' the basal plane perpendicular to the rotational plane of the magnetic field, Fig. 4c. For rotating magnetic fields, the orientation rate θ now depends also on $\omega_m = \frac{d\varphi_m}{dt}$ the frequency of the magnetic field as:

$$\frac{d\theta}{dt} = \frac{d\varphi_m}{dt} - \frac{d\varphi_p}{dt} \tag{26}$$

Thus, using equation (24) equation (26) can be rewritten as [51]:

$$\frac{d\theta}{dt} = \frac{d\varphi_m}{dt} - \frac{d\varphi_p}{dt} = \omega_m - \omega_c \sin 2\theta \tag{26}$$

Three rotating magnetic field - nanoparticle interactions are possible depending on the frequency of the rotating magnetic field, ω_m, in relation to a critical frequency, ω_c. If $\omega_m < \omega_c$ the particle becomes synchronized with the external magnetic field, and its phase remains constant over time ($d\theta/dt = 0$), i.e., phase locking. For $\omega_m > \omega_c$, phase-ejection occurs whereby a planar orientation of the nanoparticles is achieved.

3.2. Alignment techniques using static magnetic fields

Graphene nanosheet alignment using a static magnetic field is a simple and cost-effective technique. To perform the orientation, graphene dispersed in a matrix/solvent is subjected to the magnetic field for a system-specific (combination of material and magnets) orientation time. The orientation time depends upon the magnetic field strength, filler susceptibility, and the viscosity of the fluid in which graphene is orienting, see equation (25). Due to the non-uniform magnetic field generated by a single magnet, dual magnet systems are preferred for creating magnetic field induced alignment. Graphene nanosheets oriented using a dual static magnet system (Fig. 6c) have been shown to have high orientation compared to a single static magnet system (Fig. 6a). Using an electromagnet, a static magnetic field can be generated that could be used to align graphene samples even at higher magnetic field strength compared to permanent magnets (Fig. 6e). For graphene alignment solenoids type of electromagnets are used. These electromagnets are consistent with a coil of wire wound around a core. When an electric current passes through the coil, it generates a magnetic field along the axis of the coil (Fig. 6e). By placing graphene nanosheets within the magnetic field, they can be oriented and aligned in a specific direction.

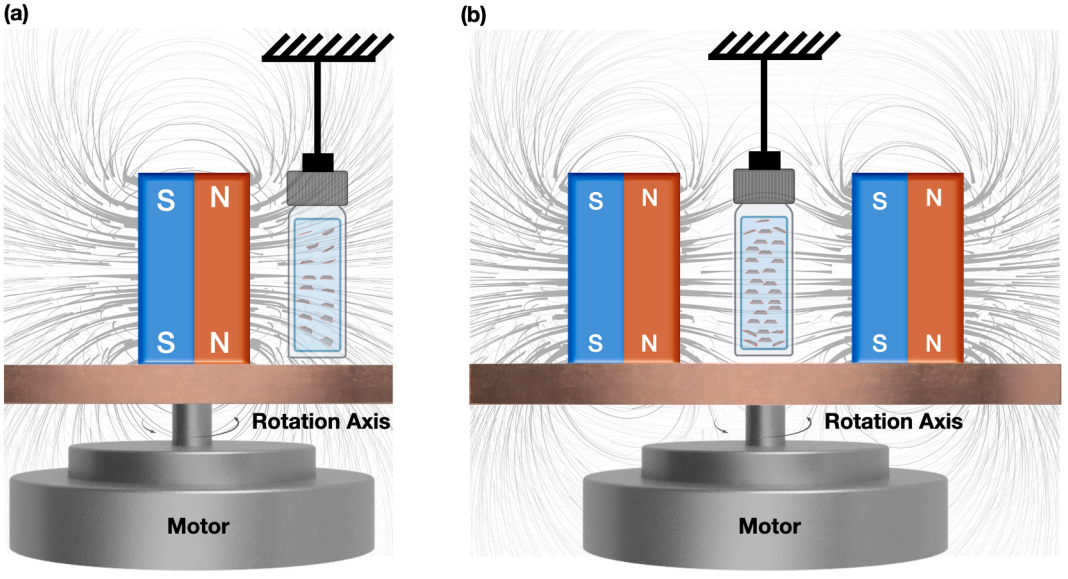

Fig. 7. Orientation technique using a permanent rotating magnetic field (a) single and (b) dual magnet system.

When graphene is aligned without ferromagnetic particles, it requires more than a 10 T magnetic field; electromagnets generate this ultrahigh magnetic field (more than 7 T) to orient diamagnetic graphene sheets [102,103]. Further, a static magnetic field could potentially fabricate composites with aligned graphene for large-scale applications [104].

3.3. Alignment techniques using rotating magnetic fields

As outlined both phenomenologically and theoretically in the previous sections, achieving alignment of oblate spheroids such as graphene nanosheets is complicated by having two degrees of freedom, in contrast to e.g., prolate ellipsoids (1D nanoparticles) [105]. Therefore, the nanosheets will still be free to rotate around the applied field line, see also Fig. 6a. Therefore, to achieve a planar alignment, i.e., aligning the plane of each disk-like structures parallel to each other, a static magnetic field is not sufficient.

To achieve a planar alignment in 2D nanoparticles, a rotating magnetic can be used (Fig. 6b and d). The aligned 2D nanostructure can be fabricated using permanent magnets in both single and dual configurations (Fig. 7). A setup for a single magnet rotating magnetic field, Fig. 7a, typically consists of a magnet driven by a motor with the rotation axis perpendicular to the table. The sample is placed next to the magnet and the graphene is aligned in the direction of applied magnetic field. However, as explained above, due to a more uniform magnetic field in a dual magnetic system, one can achieve a better orientation than in a single magnetic system. A typical setup construction is presented in Fig. 7b, where a motor drives two magnets attached to the table forming a dual magnet configuration. Further, sample is placed in the middle of the magnets for alignment. Dual magnet system as shown in Fig. 7b has more uniform magnetic field compared to single magnet. Moreover, to achieve an enhanced planer alignment in a dual magnetic field Lin et al. observed that a minimum critical frequency ω_c of 5 revolutions per second was required [105]. Enhanced planar alignment was further confirmed by researchers for several other materials [106,107]. In addition, 2D SAXS, Raman, AFM and XRD data confirmed the planar alignment of nanosheets with magnetic field rotation [70,71,108]. It has been demonstrated that aligned graphene sheets influence light propagation. Samples oriented with a rotating magnetic field have more transmission compared to samples prepared with a static

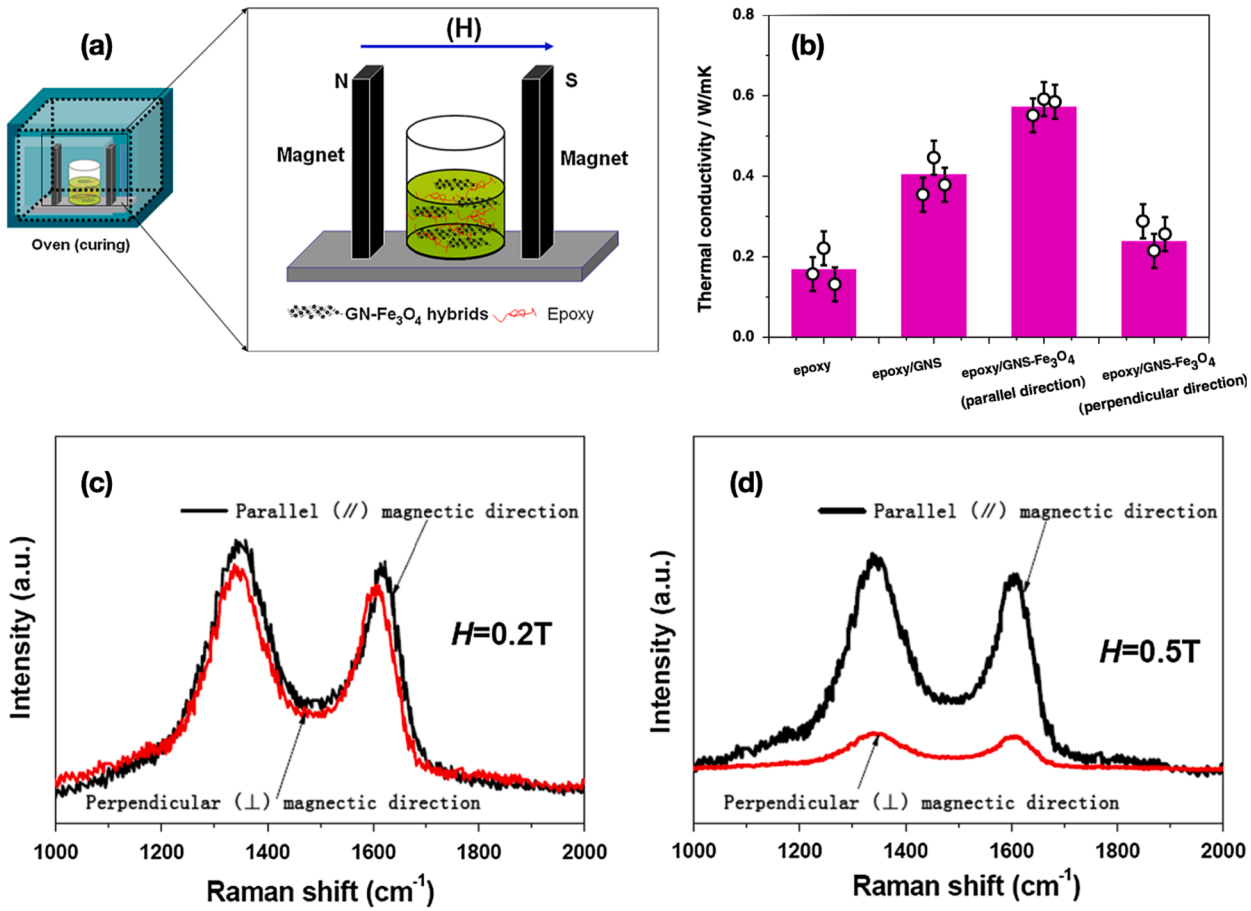

Fig. 8. (a) Schematic for the synthesis of aligned rGO@Fe_3O_4 composite under magnetic field,[80] (b) Thermal conductivity of rGO@Fe_3O_4 aligned and neat epoxy composite. a,b) Reproduced with permission [80]. Copyright 2014, Springer Nature. (c) Polarized Raman spectra for rGO@Fe_3O_4 composite aligned parallel and perpendicular to the magnetic field (0.2 T) [28], and (d) Polarized Raman spectra for rGO@Fe_3O_4 composite aligned parallel and perpendicular to the magnetic field (0.5 T). (c,d) Reproduced with permission [28]. Copyright 2014, Springer Nature.

magnetic field keeping other conditions constant [105]. Planar alignment has shown high potential for microwave absorption, antibacterial coatings and electrically conductivity composites developed with hybrid networks under a rotating magnetic field [70,71,108]. However, the implementation of rotating magnetic techniques is generally limited in terms of large-scale applications due to high rotational speed (>500 rpm) involved in the process. Therefore, it is extremely challenging to control the process. Specialized equipment and significant energy consumption further hinder the scalability of this approach. Possible solutions involve developing advanced techniques, controlled environments, and alternative alignment methods. However, rotating magnetic fields do offer superior alignment order and a uniformly dispersed graphene within composites when compared to static magnetic fields. The latter may provide lower alignment order but can be more readily employed for the large-scale production of aligned composites due to easy handling and low energy consumption.

4. Graphene alignment using magnetic fields and resulting material properties

In the following sections we focus on the properties of the materials induced through the orientation of graphene nanosheets with magnetic fields. The orientation of graphene sheets is usually referred to as vertically or horizontally orientated. While the 'horizontal' and 'vertical' designations are rather ambiguous, it is implicitly considered that given a reference plane with a normal $\boldsymbol{n}_r$, if the angle to the normal of a graphene nanosheet, $\boldsymbol{n}_G$, is 0° then the orientation in 'horizontal' while at 90° the orientation is 'vertical'. Note that the definition of the reference plane is entirely arbitrary.

4.1. Graphene alignment with ferromagnetic particles using permanent magnets

Several researchers have deposited ferromagnetic/superparamagnetic particles on graphene to achieve various desired properties for their application in different fields. The use of graphene decorated with superparamagnetic particles for alignment was first reported by He et al. [43]. The work focused on developing a single-step method for GO reduction and the adsorption of Fe_3O_4 (average size 6.3 nm) nanoparticles. The developed rGO@Fe_3O_4 nanosheets dispersed in N, N-dimethyl formamide (DMF) were placed in an external magnetic field to obtain horizontally aligned nanosheets. It has been reported that agglomeration of graphene sheets can be reduced by doping with superparamagnetic particles in both solvents and matrix; however, there are several contradictions found; further studies are required for a better understanding [28,43,80,109].

GO nanosheets doped with ferromagnetic nanoparticles have been orientated with a low magnetic field (9 to 50 mT) in a few seconds [50–52,110]. Doped GO nanosheets, when reduced (rGO), can also be aligned by directly evaporating molecules under magnetic field using a physical vapor deposition (PVD) system at room temperature [111]. The alignment of Fe-coated rGO microspheres using a dual system of permanent magnets in polyvinyl alcohol (PVA) was first demonstrated by Shen et al. [112]. The rGO encapsulated microspheres were prepared using the sol–gel method, and the composite was fabricated at −18 °C for 24 h. Under the external magnetic field, rGO microspheres were successfully aligned vertically and horizontally in the prepared composites. Results showed that the anisotropic magnetic conductive composite had higher electrical resistivity opposite to the orientation direction [112–114]. Vertically and horizontally aligned rGO@Fe_2O_3 paper developed by Jiang et al. using a hydrothermal process followed by vacuum filtration has shown enhanced efficiency in sensing H_2S gas [115]. Inspired by the gas sensing work using a magnetic field, Zou et al. demonstrated that an enhanced NO_2 gas sensor could be fabricated using aligned nanospheres Fe_2O_3@rGO under a magnetic field [116]. Using a similar approach, Ma et al. further demonstrated that aligned three-dimensional Fe_2O_3@SiO_2@rGO core–shell spheres have 7.96 times higher selectivity with ultrahigh sensitivity of 34.41 for 5 ppm NO_2 gas at room temperature compared to the randomly aligned sensing device [55].

Aligning Fe_3O_4 doped graphene nanosheets filler in an epoxy matrix is relevant for numerous composite applications. Yan et al., demonstrated the alignment of Fe doped graphene under an external magnetic field, as shown in Fig. 8a [80]. Magnetic nanoparticles of rGO@Fe_3O_4 were chemically synthesized by reducing GO in $FeCl_3$ and hydrazine hydrate solution. The prepared nanoparticles had 66.7 wt% of Fe_3O_4 and 1 vol% of rGO@Fe_3O_4 was used to fabricate composites in a 0.3 T magnetic field. The fabricated nanocomposite showed a 140 % increase in thermal conductivity in the aligned direction compared to neat epoxy, as shown in Fig. 8b. Other groups also observed a similar trend in another work, where 0.52 vol% filler (rGO@Fe_3O_4) content at 0.5 T magnetic field showed a 111 % and 48 % higher thermal conductivity than neat epoxy and non-aligned epoxy composite, respectively [28,117]. In addition, the degree of orientation in the fabricated nanocomposite was evaluated using polarized Raman spectroscopy [118]. It was observed that the Raman peak intensity has a high sensitivity towards the variation in graphene alignment [28,80,119,120]. The graphene aligned parallel to the polarized laser excitation showed an enhanced intensity compared to perpendicularly aligned graphene nanosheets in the composite. No difference in the Raman peak intensity was observed at 0.2 T magnetic field due to insufficient strength to introduce alignment (Fig. 8c) [28]. However, a significant difference in the intensity was observed when graphene sheets were aligned at a 0.5 T magnetic field, as shown in Fig. 8d [28].

Geng et al. showed that with 30 wt% aligned filler (rGO@Fe_3O_4) in an epoxy matrix, thermal conductivity could be enhanced by more than 196.6 % compared to pure epoxy composite [48]. Yoonessi et al. demonstrated that Ni could provide highly aligned graphene composites like Fe-doped composites due to their superparamagnetic properties [49]. The solvent casting method was used for composite fabrication, 1.3 vol% rGO@Ni nanoparticles were added to polyimide and placed under a magnetic field of ≈1 T. Fabricated aligned composite showed higher mechanical and electrical properties than non-aligned composite. With 2.5 times higher in-plane DC conductivity and a 2-fold increase in tensile strength, the enhanced horizontal alignment of rGO@Ni in polyimide was established. Moreover, the orientation of rGO@Ni in polyimide was further confirmed with saturation remanent magnetisation (M_r). The measurements showed that the fabricated composite had M_r maxima at 0° and 180° in the horizontal direction (parallel to the

magnetic field) and minimum M_r at 90° and 270° [49]. In a similar work by Hu et al., a hybrid of GO-CNT@Ni filler was fabricated using the molecular-level-mixing method [83]. The prepared fillers were added to an epoxy matrix and aligned under a magnetic field. The alignment verified using SEM and XRD showed 2.7 times higher thermal conductivity and 10^4 times better electrical conduction performance than pure epoxy. Pisharam et al. have reported the enhancement of EMI shielding capability (127 %) along with excellent electrical conductivity (more than 5 orders of magnitude) of nickel ferrite ($NiFe_2O_4$) doped graphene filler in epoxy when aligned under a low magnetic field (0.167 T) [120]. In another work Li et al., showed that aligned Fe-doped rGO nanosheets in a poly(propylene carbonate) composite could enhance EMI shielding along with thermal conductivity (135 %) under a low magnetic field (0.2 T) [72]. Horizontally aligned Fe_3O_4 doped rGO composites membranes in pyrrole showed promising application as a glutathione sensor [121]. In addition, it was found that aligned graphene@Fe_3O_4 fillers mixed in different polymers can be used to enhance proton conductivity, thermal stability and water intake capacity; therefore, these composites find huge applications for effectively suppressing methanol permeation in a fuel cell [63,66,67,122]. Prevention of food from degradation during transport, storage and sales are one of the biggest contemporary global challenges. A packaging material developed by horizontally aligned graphene nanosheets composites could provide a sustainable and economically viable solution [67,69]. Horizontally aligned and congregated nanocomposites films produced by adding (0.072 vol%) GO@Fe_3O_4 fillers to PVA under an external magnetic field by Ren et al. showed enhanced gas barrier properties (low O_2 permeability, 99 % compared to pure PVA) with high mechanical strength and thermal stability [69]. However, the produced films showed two different regions: the aligned and congregated GO@Fe_3O_4 region and the pure PVA region. The presence of two regions in the films might be due to the non-uniform magnetic field applied only from the single side of the prepared films, which has the potential to be improved by using a dual magnetic system. In another study, Zhu et al. demonstrated that (3 wt%) GO@Fe_3O_4 fillers aligned in the Pebax matrix can efficiently separate CO_2 from a mixture of CH_4 or N_2 that could have a significant potential to control greenhouse gas emissions [64]. The vertically aligned Fe-doped GO sheets provide a shorter path to CO_2, leading to 113 % enhanced CO_2 permeability compared to morphology having random filler orientation. The use of vertical alignment was further demonstrated by Renteria et al. showing the adsorption of negatively charged Fe nanoparticles on positively charged graphene nanosheets, which were aligned vertically in epoxy under an external magnetic field of 1.2 T [78]. The prepared composite with vertically aligned graphene nanosheets showed a factor of 2 improvement in thermal conductivity (1.25 W/mK) compared to the randomly orientated composite (0.6 W/mK). Moreover, the prepared composite successfully reduced the temperature of a commercial CPU (Intel® Core™ i7-4770K) by 10 °C (4 wt% filler), demonstrating the potential of vertically aligned graphene sheets as a thermal interface material [78]. To further enhance the thermal conductivity, Li et al. fabricated a novel filler of carbon nanotube (CNTs) grafted graphene polyhedral (Co@Co_3O_4-G) [81]. It has been shown that during the carbonization process, CNTs and graphene layers are formed by the catalysis of reduced Co nanoparticles as shown in Fig. 9. The fabricated filler (8.7 vol%) showed excellent thermal conductivity (2.11 $Wm^{-1}K^{-1}$) in the epoxy matrix due to the formation of conductive paths when aligned under the magnetic field [81]. In a similar work by Xu et al., a graphene-coated ultrafine cobalt nanoparticles-based porous metamaterial was fabricated under a magnetic field [82]. The aligned 3D structure showed potential to be used for electrochemical water splitting. However, a percolated filler network is required to achieve ultra-high thermal conductivities. Therefore, He et al. developed a filler by doping graphene with Fe and SiC nanowires (graphene@Fe/SiC) [123]. Further, the fabricated filler was aligned vertically using a magnetic field in an epoxy matrix and showed a 311.6 % enhanced thermal conductivity compared to pure epoxy [123]. Vertically aligned graphene as an electrode for next-generation batteries is very promising due to the high surface area of graphene nanosheets. Serradet et al. demonstrated that sulfonated graphene (G_S) decorated with Fe nanoparticles could be vertically oriented on a gold surface (in

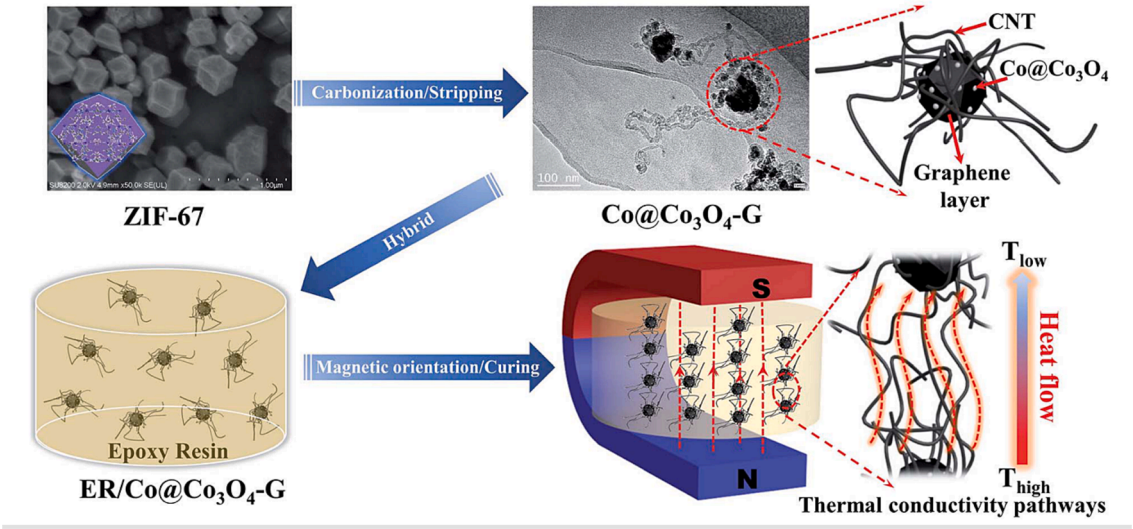

Fig. 9. Schematic showing the preparation of Co@Co_3O_4-G filler and final composite under magnetic field. Reproduced with permission [81]. Copyright 2020, Royal Society of Chemistry.

methanol) using an external magnetic field of 1.2 T. Cyclic voltammetry results further confirmed orientation with an increase of 117 % in the current of vertically oriented G_S@Fe on a gold surface compared to neat Au electrode [124]. Graphene having a large surface area and high thermal conductivity showed excellent wear-resistance properties when aligned in a composite using an external static magnetic field [68,109]. Liu et al. demonstrated that composites made by aligned rGO@Fe_3O_4 filler in Bismaleimide (BMI) exhibit excellent mechanical and tribological properties [68]. The fabricated composite consisted of 0.6 wt% horizontally aligned rGO@Fe_3O_4 and showed a 23.4 % and 14.7 % increase in flexural and impact strength, respectively. Tribological studies showed an 85 % decrease in wear rate of the aligned composites compared to neat BMI, with a low friction coefficient of 0.07 [68]. In another study by the same group, polyphosphazene was attached to fillers to form rGO@Fe_3O_4polyphosphazene and thus improve compatibility and interfacial adhesion between rGO@Fe_3O_4 and BMI matrix [109]. The fabricated aligned composite showed enhanced mechanical (54.5 % impact strength) and tribological (friction coefficient 0.09, volume wear rate 93.5 %) properties and improved thermal stability compared to neat BMI [109]. In both these studies, it was found that horizontally aligned graphene acts as a self-lubricating film leading to very mild wear (abrasive wear mechanism) compared to the neat BMI having a high wear rate (with both adhesive and fatigue wear mechanism). Therefore, it was established that the horizontally aligned graphene in the composite reducesfriction and improves anti-wear capacity [59,68,109].

Percolated aligned graphene in a polymer forms conductive paths for electron flow, enabling semiconductive applications. Ding et al. prepared rGO@Fe_3O_4 filler by reducing GO and attaching Fe nanoparticles using a hydrothermal process [57]. The prepared filters were aligned vertically, horizontally, or randomly using an external magnet (0.6 T) to study dielectric properties. It was demonstrated that horizontally aligned composite (10 wt% filler content) had 355 times, 9.4 times, and 21 times higher dielectric constant than pure polyimide, randomly oriented and vertically oriented composite, respectively [57]. This high dielectric constant in horizontally aligned composite was due to the presence of graphene sheets parallel to the film and stacked layer by layer in a sandwich form leading to the formation of nanocapacitors, causing more charge accumulation compared to the vertically aligned graphene nanosheets, which will have charges present only on the terminal surfaces [57].

Graphene nanoplatelets (GNPs), due to fewer oxygen-containing functional groups, provide excellent mechanical and electrical properties compared to GO when aligned in a polymer composite [125]. Aligning Fe decorated GNPs@polyvinylpyrrolidone filler in epoxy was demonstrated by Wu et al. using a weak magnetic field (0.02 T) [52]. Results showed that the composite fabricated using 1 wt% filler can be rotated from 89° to 1° in ~9 min in epoxy with a viscosity of 2.7 Pa·s. It was found that the filler alignment time depends upon the initial angle of the filler, the magnetic field applied, the viscosity of the suspension and the volume fraction of filler in

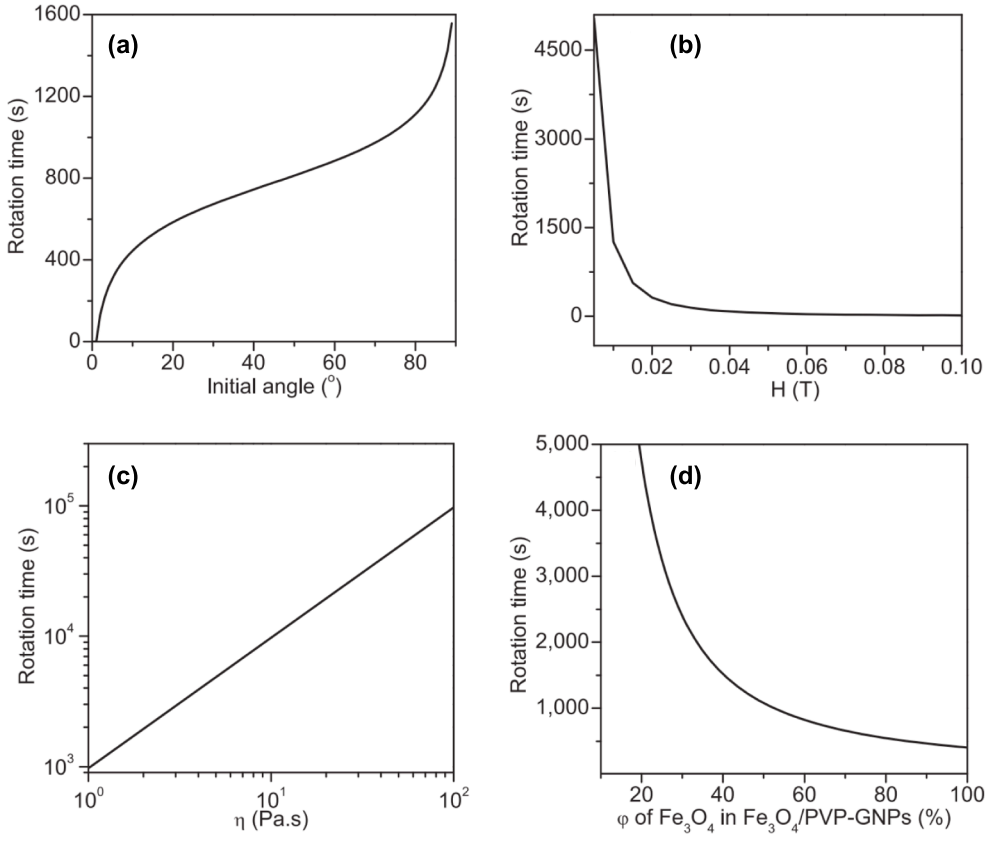

Fig. 10. GNPs-based filler rotating time as a function of (a) initial angle of filler, (b) magnetic field applied, (c) viscosity of the suspension and (d) filler volume fraction. Reproduced with permission [52]. Copyright 2016, Elsevier.

the composite, as shown in Fig. 10 [52]. In addition, the developed GNPs-based composite showed a 50 % enhancement in fracture energy and a seven-fold increase in electrical conductivity in the aligned direction [52].

Yao et al. fabricated a solvent-free aligned composite using a similar low viscosity epoxy.[126] The fabricated composite consisted of a filler of CNTs and GO decorated with Fe_3O_4 nanoparticles. The filler was further covered with polyether to increase dispersion and reduce agglomeration in epoxy when aligned at a magnetic field of 0.6 T. Results showed that aligned composite with 1 wt% filler had enhanced mechanical (136.5 % improvement in impact strength and 30.9 % bending strength) and thermal properties compared to the neat epoxy.[126] In another work, Chaichi et al. used GO@Fe_3O_4 fillers in PVA to fabricate aligned nanocomposites, demonstrating that the alignment has no significant effect on PVA crystallization.[127] However, even with the addition of aligned 0.1 wt% fillers in PVA using a weak magnetic field of 0.075 T can lead to a significant enhancement in mechanical properties (63, 143, 162 % increase in the modulus, tensile strength, and toughness, respectively) of the composites compared to neat PVA.[127].

With the rise in the earth's temperature, the drastic effects of global warming are now visible in terms of decreasing freshwater resources. Therefore, research on water purification and desalination systems has been focused on as never before. Using the knowledge of aligning Fe-doped graphene, Huang et al. developed a polyvinylidene fluoride (PVDF) based membrane with GO@Fe_3O_4 fillers under a magnetic field of 0.05 T.[53] The fabricated membrane with 1 wt% GO@Fe_3O_4 (72.5 wt% Fe_3O_4 and 24.8 wt% GO) fillers aligned vertically showed high pure water flux with a flux recovery ratio of 83 %, which means the foiling in the membrane can be quickly cleared by washing. The addition of aligned hydrophilic GO@Fe_3O_4 in membrane fabrication helps not only in the increase of water flux but also in the antifouling properties of the membrane compared to the pristine hydrophobic PVDF membrane.[53] Designing a functionally aligned tissue would potentially benefit in treating many chronic diseases of the central nervous system, such as neurodegenerative diseases and traumatic brain injuries [128]. To this end, Santhosh et al. 3D printed a collagen-based hydrogel using rGO@Fe filler under a magnetic field (0.05 T) [74]. The developed 3D scaffold showed the growth of aligned neuronal stem cells (with rGO@Fe) and enhanced differentiation of neurons. In addition, the differentiated neurons in hydrogel showed unidirectional calcium signal propagation along the alignment [74]. Kukhta et al. developed a composite using poly(3,4-ethylenedioxythiophene): polystyrene sulfonic acid as a matrix and GNP@Fe_3O_4 as a filler under a magnetic field (0.15 T). The weight ratio of polymer to filler (GNP@Fe_3O_4, 60:40 wt ratio) was 1:1 in the composite. During composite fabrication a magnetic field applied perpendicular to the film leads to the vertical alignment of filler [129]. It was observed that the alignment of fillers was not perfectly perpendicular to the film, and more study is required for better understanding. However, Shi et al., using GNP@Fe_3O_4, showed better alignment without any porosity in the silicon rubber matrix. XRD and SEM further confirmed the alignment of GNPs in silicon rubber, which showed an enhanced thermal conductivity (191 %) at 5 wt% of filler content compared to randomly composite [79]. Dong et al. developed GNPs@CIPs (Carbonyl iron particles) filler and aligned in polydimethylsiloxane (PDMS) under a magnetic field of 0.5 T. The developed composite showed a significant reduction in percolation threshold for aligned composite (0.15 vol%) compared to unaligned composite (0.85 vol%) due to the formation of the conductive network [76]. A similar work by Lui et al. showed GO@Fe_3O_4 nanorods, when added with boron nitride in a polyimide-based composite and aligned horizontally under a magnetic field of 24 mT, enhanced the in-plane thermal conductivity by more than 1233 % compared to pure polyimide composite [104]. Even though the developed method has the potential for large-scale production, orientation in the composite suffers due to the use of a single magnet system.

Despite the progress reported, most composites developed with aligned GnPs lack or partially loose orientation after fully cured. Therefore, Wu et al. studied the effect of curing GNP@Fe_3O_4 filler in epoxy; it has been demonstrated that alignment could be improved with rapid curing methods (e.g. UV-triggered frontal polymerization) compared to thermal curing [75]. With the rapid curing method, the thermal conductivity of fabricated composites increased by 53 % with 2 wt% GNPs under a 5 T magnetic field [75]. Younes et al. used a similar UV-curing method to align GNPs@Fe_3O_4 filler in a polymer composite when 3D printed [77]. The composite aligned at 0 degrees showed enhanced Young's modulus compared to a 90° aligned composite under a static magnetic field [77].

Designing transparent and electrically conductive graphene-based multifunctional composites finds significant potential as a transparent electrode for photovoltaics, smart windows and other optoelectronic devices [61,130,131]. To realize this, Ferrand et al. demonstrated for the first time that Fe adsorbed on GO when reduced to rGO for, can be oriented in both static and rotating magnetic fields [70]. The horizontal and vertical alignment of rGO in gelatin and poly(2-acrylamido-2-methyl-1-propane sulfonic acid) (PAMPS) has been confirmed using wide and small X-ray scattering measurements. The designed thin films of rGO-based hydrogel, when aligned in a 2D network, showed 80 % transparency. In addition, the aligned structure forms a local percolating network at 0.75 vol%, leading to high electrical conductivity. In another work, Zheng et al. demonstrated that graphene oxide conjugated with gold nanoclusters when doped with paramagnetic holmium ions could be oriented in a magnetic field. The vertically oriented GO sheets showed 99 % antibacterial efficacy against both gram-positive and gram-negative bacteria [132].

The alignment of Fe-doped graphene using a rotating magnetic field could open new possibilities for various applications, including microwave absorption as demonstrated by Liu et al. and Dai et al. [71,135]. Results showed that even 2 wt% of aligned rGO@Fe_3O_4 filler in waterborne polyurethane composite can lead to a minimum reflection loss of −67.8 dB, further confirming the aligned rGO in the matrix [71]. In a similar work, Fu et al. demonstrated that 1D Fe_3O_4 nanowires could be chemically synthesized using dopamine [58]. The synthesized 1D nanowires, when attached to the basal plane of rGO, showed enhanced gas barrier along with ultra-high electromagnetic interference (EMI) shielding and microwave absorption capability when aligned under a magnetic field of 35 mT. A 2 wt% rGO@Fe_3O_4 nanowires aligned vertically to the incident wave in an epoxy matrix showed 99 % effective absorbance compared to horizontally aligned, showing 68 % microwave absorbance [58]. In addition to this, Shemshadi et al. demonstrated that under a magnetic field rGO@Fe_3O_4 (0.5 wt%) could be oriented in a polyacrylamide matrix [56]. The oriented composite finds potential application in the field of moisture and heat management due to its enhanced capability compared to the randomly oriented composite counterpart. In a similar work, Hong et al. demonstrated that rGO grafted with Fe nanoparticles could be aligned under a

magnetic field in both horizontal and vertical directions [73]. They showed a 250 % improvement in EMI shielding in aligned samples compared to random samples. However, they specifically mentioned the issues of using the dual magnetic system, which does not align graphene sheets completely due to the non-uniform magnetic field it possesses [73]. Ding et al. [136] showed that the horizontally

Table 2
Ferromagnetic particles adsorbed graphene nanosheets in a magnetic field, and the potential applications.

Product	Material/fillers	Magnetic Field Alignment	Composite Properties	Application	Reference
G_S@Fe_3O_4 is mixed in sulfonated poly ether ether ketone (SPEEK) and fluorinated poly arylene propane biphenyl (FPAPB)	Different wt. % of filler is added to a composite of SPEEK (90 %) and FPAPB (10 %) and cured under a magnetic field	0.25 T V	The synthesized aligned composite showed enhanced proton conductivity, thermal stability, and water intake capacity with a low O_2 and H_2 permeability	High-temperature and low-humidity fuel cells and has gas barrier properties	Vinothkannan et al. (2017)[67]
Negatively charged Fe is adsorbed on positively charged graphene to produce magnetic filler	1 wt% filler is added to epoxy under an external magnetic field	1.2 T V	The thermal conductivity of an aligned composite is two times higher than non-aligned composite.	Thermal interface material	Renteria et al. (2015)[78]
G_S@Fe deposited on gold substrate using magnetic field	100 μL G_SO@Fe dispersed in DMSO are added dropwise to gold substrate submerged in methanol	1.2 T V	Current collection increases to 3.5-fold in aligned composite used as electrode compared to Au_pt electrode	Electrode for batteries, and sensor	Serradet et al. (2016)[124]
GO is reduced to form rGO@Fe_3O_4 in the presence of $FeCl_3$ and hydrazine hydrate solution.	0.6 wt% filler is added to bismaleimide (BMI) under an external magnetic field	0.2 T H	The aligned composite showed 23.4 % and 14.7 % increase in flexural and impact strength, respectively. Tribological studies showed 85 % decrease in wear rate with a low friction coefficient of 0.07 of the aligned composites compared to neat BMI	Coatings for low wear rate	Liu et al. (2015) [68]
GO@Fe_3O_4 filler is prepared chemically and added to polyvinylidene fluoride for membrane fabrication	1 wt% filler is added to polymer under external magnetic field	0.05 T V	Fabricated membrane provides a high pure water flux of 484 $Lm^{-2}h^{-1}$ along with high flux recovery ratio of 83 %	Membrane for water	Huang et al. (2018)[53]
Fe is adsorbed on graphene to produce magnetic filler. The filler is added to collagen hydrogel	0.1 mg/ml filler in hydrogel is 3D printed to form a scaffold for aligned cell growth	0.05 T –	growth of aligned neuronal stem cells and enhanced differentiation of neurons	3D printed Scaffold	Santhosh et al. (2019)[74]
Fe is chemically attached on GO and reduced to synthesis rGO@Fe_3O_4 and added to waterborne polyurethane (WPU) as a matrix	Composite is prepared by mixing 2 wt% filler (rGOFe_3O_4) in WPU matrix	0.9 T H	Aligned composite showed enhanced microwave absorption capacity. With a 2 wt% filler the minimum reflection loss observed are −67.8 dB.	Microwave Absorption	Dai et al. (2019) [71]
GO@Fe_2O_3 nanoparticles mixed in polymer to form composite	0.8 wt% of filler is added to polymer and 3D printed followed by UV-curing.	0.03 T H	Aligned sample having 0.8 wt% filler showed enhanced young's modulus compared to pure composite.	Mechanical Properties	Younes et al. (2022)[77]
GO-CNT@Ni filler is prepared and added to epoxy	30 wt% filler is added to epoxy matrix	0.05 T V	Aligned composite showed enhanced thermal and electrical conductivity of 2.4 times and 10^4 times higher compared to pure epoxy	Thermal and electrical conductivity	Hu et al. (2022) [83]
Fe_2O_3@SiO2@rGO core shell spheres are fabricated chemically	Fe is fabricated chemically and coated on SiO_2 spheres and further a coating of GO is attached chemically	0.28 T H	Aligned device showed 7.96 times higher selectivity with ultrahigh sensitivity of 34.41 for 5 ppm NO_2 gas at room temperature compared to the randomly aligned sensing device.	NO_2 Sensor	Ma et. al (2020) [55]
GO@Fe_3O_4 filler is prepared chemically and added to waterborne epoxy	60 wt% filler is added to epoxy for composite fabrication under magnetic field	– H	Aligned composite showed a significant reduction in diffusion and penetration of corrosion media.	Corrosion Resistance	Wang et al. (2020)[133]
GO + Nafion is drop casted on electrode	1:1 ratio of graphene@Fe and Nafion are deposited on electrode	0.4 T V	–	Glucose Sensor	Yin et al. (2021) [134]
Holmium doped GO conjugated with gold nanoclusters is added to polymer.	Holmium doped GO (4 mg/ml) is aligned in magnetic field.	0.5 T V, H	Vertically aligned composite showed enhanced (99 %) antibacterial efficacy.	Antibacterial activity	Zheng et. al. (2018)[132]

aligned GO@Fe_3O_4/Zn in epoxy could provide better corrosion resistance coating. Comparable results were observed by Wang et al., indicating a significant reduction in diffusion and penetration of corrosion media by horizontally aligned graphene nanosheets [133]. In a similar work by Lei et al. the anti-corrosion capability of aligned GO@Fe_3O_4@SiO_2 filler in the epoxy matrix is studied [62]. It was observed that SiO2 form GO@Fe_3O_4 filler is superhydrophobic when coated chemically. The developed superhydrophobic filler, when aligned horizontally in epoxy using permanent magnets, makes enhanced transparency (94 %) and anti-corrosive capability (43 times higher resistance) compared to pure epoxy [62]. Several researchers have demonstrated that the GO@Fe_3O_4 filler in the matrix, when aligned under a magnetic field, could influence the performance of several applications. However, Shen et al. showed for the first time that the mechanical properties of aligned composites also improve significantly compared to the random composites [137]. It has been found that the interlaminar shear strength, tensile strength, and flexural strength of the aligned composite enhanced by 41 %, 29.7 %, and 40.9 %, respectively [137]. Sensing glucose is highly required these days due to the increased number of diabetic patients worldwide. Yin et al. demonstrated that vertically aligned graphene@Fe + Nafion coating on electrodes in a constant magnetic field (0.4 T) had shown a potential to analyze glucose in human serum samples [134]. In another work, Park et al. demonstrated the potential of GO@Fe_3O_4 foam prepared by orienting in the magnetic field [65]. The prepared foam, having aligned graphene sheets, not only showed fascinating origami architectures but also had enhanced surface area and mechanical properties. Various applications of differently prepared graphene@ferronanoparticles have been summarized in Table 2. Essentially, magnetic induced orientation using

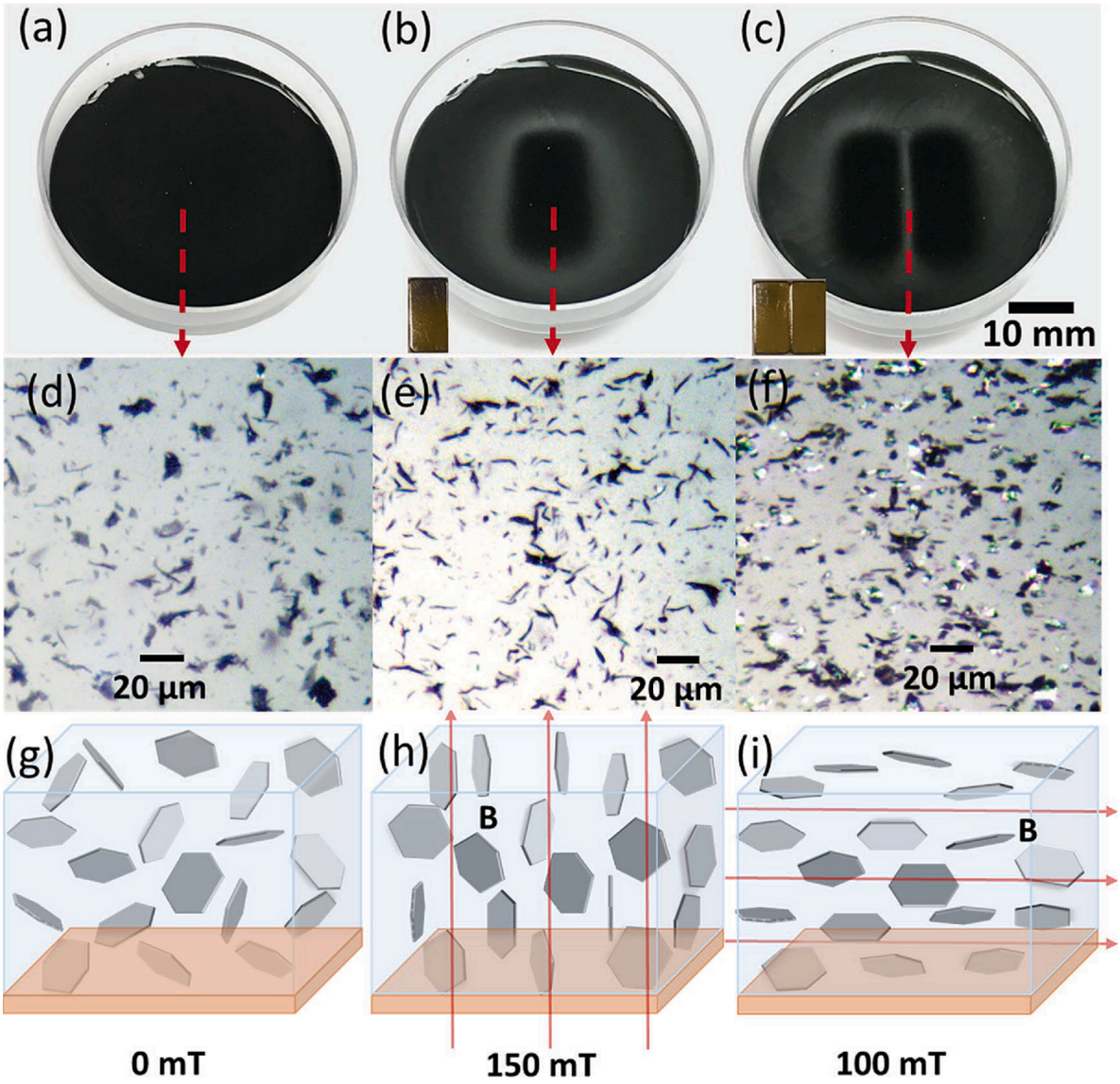

Fig. 11. Showing optical reflectivity variations due to the applied magnetic field (a-c) Optical images with graphene suspension when zero, one and two magnets are placed (d-f) optical microscopic images of graphene samples oriented under static magnetic field (g-i) schematic showing graphene flake orientation under a static magnetic field. Reproduced with permission [86]. Copyright 2016, Wiley-VCH.

permanent magnets with the aid of ferromagnetic nanoparticles magnets has been demonstrated for all graphene types. Fe_3O_4 is the most used ferromagnetic nanoparticle with a relatively broad range of magnetic fields applied, 0.05, 1.2 T. Some polymer matrix/filler formulations have allowed for the orientation of rather high filler contents (up to 60 wt%), some with relatively low magnetic fields, 30 wt% using 0.05 T. Remarkably, within the range of graphene derivatives, ferromagnetic nanoparticles, concentrations and magnetic fields, magnetic field orientation has been shown to potentially impact a broad variety of applications.

4.2. Graphene alignment without ferromagnetic particles using permanent magnets

Graphene, a diamagnetic material at room temperature, requires high magnetic fields without ferromagnetic/superparamagnetic particles for orientation. This corresponds to materials having magnetic susceptibility in the range of 10^{-8}–10^{-10} emu/g [36]. Ominato et al. showed theoretically that at least a 9 T magnetic field is required at 300 K to orient graphene nanosheets [102]. It was observed that because of the diamagnetic ring current effect of their π-conjugated systems, graphene sheets have high susceptibility in the orthogonal direction to their planes. Due to this high susceptibility, the diamagnetic graphene sheets are oriented in the ultra-high magnetic field (9−16 T) [138,139]. GO orientation in composites in vertical and horizontal directions was confirmed using 2D SAXS, XRD, and Raman spectroscopy [108,138,140–143]. Xu et al. demonstrated that defects such as valency, zigzag edges, and adatoms in graphene nanosheets develop local magnetic moments by forming unpaired spins leading to anisotropic magnetism; therefore, the magnetic field requirement reduces drastically [41,42,50]. Inspired by this work, Takahashi et al. demonstrated that graphene could be aligned at a lower field strength than the minimum theoretical value [36]. The group showed that graphene's high susceptibility in one axis, being much higher than another, could be used to orient rod-like β-Si_3N_4 particles in a low magnetic field (0.4 T) [36]. It is observed that the thermal conductivity of graphene-coated β-Si_3N_4 particles varies drastically when aligned in parallel (96 $Wm^{-1}K^{-1}$) and normal (64 $Wm^{-1}K^{-1}$) to the direction of the applied magnetic field [36]. In another work, He et al. observed a strong magnetic response from fluorinated graphene nanosheets when photoexcited (325 nm) under a 900 mT magnetic [45]. It has been further demonstrated that the dielectric constant of solvents carrying graphene strongly influences the magnetic response.

In another work, Smarzewska et al. demonstrated that a uniform magnetic field (constant magnetic field, CMF) exposure on GO leads to GO sheets' activation, significantly enhancing the electroactive area when used in the sensor [146]. This enhancement in surface area is due to the change in both the surface and structure of GO under the constant magnetic field [147]. Based on Smarzewska's work, Lu et al. demonstrated that the GO could be orientated vertically using a weak magnetic field of 0.4 T leading to an enhanced electron transfer rate for an H_2O_2 sensor. Results showed that vertically aligning GO had achieved excellent selectivity and anti-interference ability in the H_2O_2 sensor [144]. Similarly, Li et al. oriented GO@Nafion vertically in CMF and showed no change in the electron transfer kinetics when the electrode was used to detect chemical oxygen demand [147].

In another work, Bie et al. demonstrated that the distance between the graphene layers could also be controlled using the magnetic field [148]. The GO liquid crystal nano papers developed under a magnetic field showed better ion transport and sieving capabilities. The application of aligned graphene membranes is demonstrated by Liu et al., where they developed a composite membrane containing an aligned G_S sheet in Nafion under a high magnetic field that showed promising potential to be used for high-performance fuel cells [98]. The developed membrane (40 μm thickness) showed high water uptake and proton-conductivity compared to pure composite. In addition to the above, the developed membrane showed exemplary performance as a gas barrier coating for hydrogen and oxygen gas [98].

The orientation of graphene using a static (Fig. 11) and rotating dual permanent magnetic system was demonstrated by the Bao group [86,105,149,150]. They showed that orientation from a dual magnetic system is more uniform than that of a single magnet due

Table 3
Graphene nanosheets aligned under a magnetic field and the potential application.

Product	Material/fillers	Magnetic Field Alignment	Composite Properties	Application	Reference
GO is coated on mesoporous silica and the solution is drop coated on an electrode	5.0 μL GO solution with Horseradish peroxide@mesoporous silica is drop casted	0.4 T V	–	H_2O_2 Sensor	Lu et al. (2020)[144]
GO + Nafion is drop casted on electrode	0.5 mg/L GO and Nafion solution	0.4 T V	–	To detect chemical oxygen demand	Li et al. (2020)
G_S is added to Nafion to form a composite membrane	Graphene loading varied from 0 to 5 wt%	1.5 T V	The aligned composite membrane showed enhanced water uptake and proton conduction	Potentially to be used in fuel cells and as a gas barrier membrane	Liu et al. (2022)[98]
GNPs are added with β-Si_3N_4 to form the composite under magnetic field	20 vol% GNPs and 80 vol% β-Si_3N_4 are mixed to form slurry which is oriented.	0.4 T V, H	Aligned composite showed enhanced thermal conductivity	Thermal Conductivity	Takahashi et al. (2016) [36]
GNPs are added to PVDF and epoxy to develop a 3 mm thick composite under a magnetic field	30 wt% GNPs are added to matrix (PVDF: EP = 1:3) and cured under a magnetic field	0.3 T H	Aligned composite showed enhanced EMI shielding along with electrical conductivity of 400 S/m	EMI Shielding	Zhou et al. (2023)[145]

to the anisotropy of graphene nanosheets. The developed system showed that a minimum of 5 revolutions per second is required under a magnetic field for fully aligned graphene nanosheets in a polymer or solvent [105]. Inspired by this Zhou et al. demonstrated the enhanced electromagnetic interference shielding capability of GNP-based composites in a rotating magnetic field (300 mT). The developed composite (30 wt% GNP) showed an electrical conductivity of 400 S/m along with an excellent EMI performance of 95 dB at a thickness of 3 mm [145]. The results of several researchers, shown in Table 3, pave the way to orient diamagnetic large-size graphene sheets in a small magnetic field without ferro/superparamagnetic material.

4.3. Graphene alignment using electromagnets

4.3.1. Graphene alignment with ferromagnetic particles

To verify the desired orientation in the composite during fabrication would provide more control to design ultra-aligned nanocomposites. To this end, Dyer et al. showed the real-time orientation of magnetic graphene nanoparticles (1 wt%) in epoxy using electromagnets (0.1 T) [151]. In another work by Zhang et al. compared GO@Fe_3O_4 filler aligned in epoxy using both electromagnetic coil and permanent magnets [60]. Orientation achieved using electromagnets demonstrated enhanced mechanical properties (6.63 % and 9.75 % improvement in impact strength and flexural modulus, respectively) due to the uniform magnetic field produced by an electromagnetic coil. Yang et al. showed that the alignment of Ni-doped GNPs in epoxy-based composites could enhance the thermal and electrical properties [84]. The increase in conductivities was attributed to the forming of a hybrid network of Ni-GNPs in epoxy under a magnetic field of 2.6 T (Fig. 12). The fabricated composite (2 wt% GNPs and 28 wt% Ni) showed 267.6 % higher thermal conductivity compared to the neat epoxy sample [84]. In another work, Liu et al. demonstrated that GO@Fe_2O_3 nanoparticles, when added to cement and oriented under a magnetic field, could enhance mechanical properties such as flexural strength and flexural modulus of elasticity of aligned composite by more than 90 % after 28 days [152].

4.3.2. Graphene alignment without ferromagnetic particles

Wu et al. demonstrated experimentally for the first time that GO nanosheets could be oriented under the magnetic field of 10 T in a hydrogel composite [140]. However, to break the degeneracy in GO nanosheets, Lu et al. used a rotating magnetic field (6 T) to achieve enhanced orientation in both vertical and horizontal directions [108]. The fabricated composite of aligned GO in 2-hydroxyethyl methacrylate (HEMA) showed enhanced antibacterial activity against *Escherichia coil (E. coli)* [108]. Further extending their work, Lu et al. demonstrated that GO could be aligned inside Polyoxadiazole-co-hydrazine to fabricate a membrane for water desalination [143]. The developed membrane with vertically aligned GO sheets exhibits an enhanced antibacterial effect (71. 7 %) against *E. coli* without affecting water permeability and salt selectivity. Li et al. showed that the thermal conductivity of GNPs in PDMS could be enhanced by aligning the fabricated composite under a static magnetic field of 10 T [142]. The proposed method showed an increase of 174 % in thermal conductivity (in the orientation direction) of the vertically aligned composite containing 3 wt% GNPs compared to pure PDMS. In another study, Lin et al. showed that vertically aligned graphene nanosheets blended with poly(3,4-ethylenedioxythiophene) aligned under a static dual magnetic system of 12 T (Fig. 13) significantly increased the charge/discharge rate and power density compared to the unaligned electrode in a supercapacitor [103]. Further, the exposed edges of vertically aligned

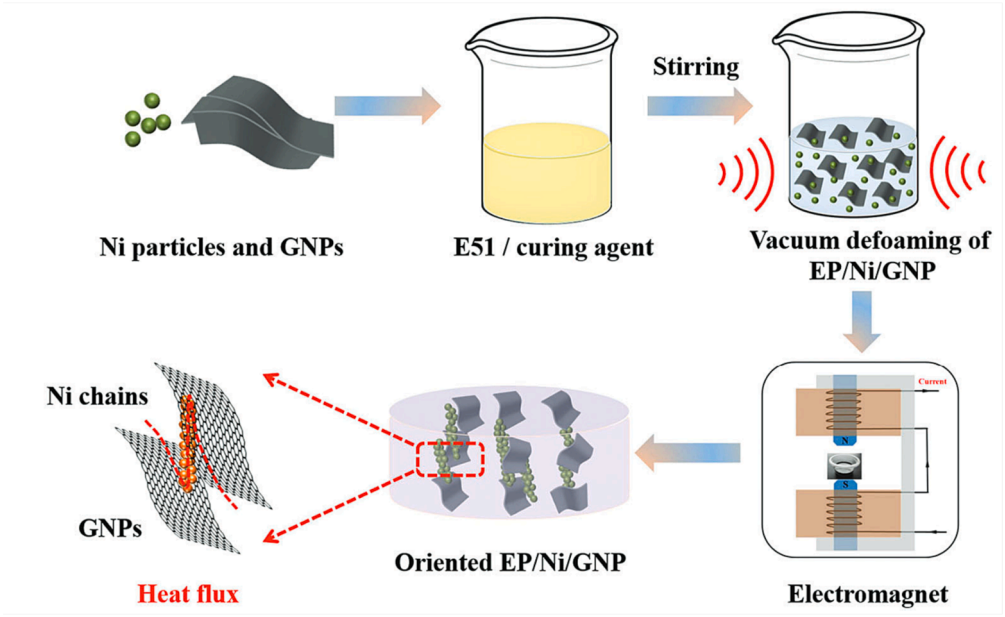

Fig. 12. Schematic showing Ni/GNPs composite fabrication and orientation process in a 2.6 T electromagnet. Reproduced with permission [84]. Copyright 2022, Wiley-VCH.

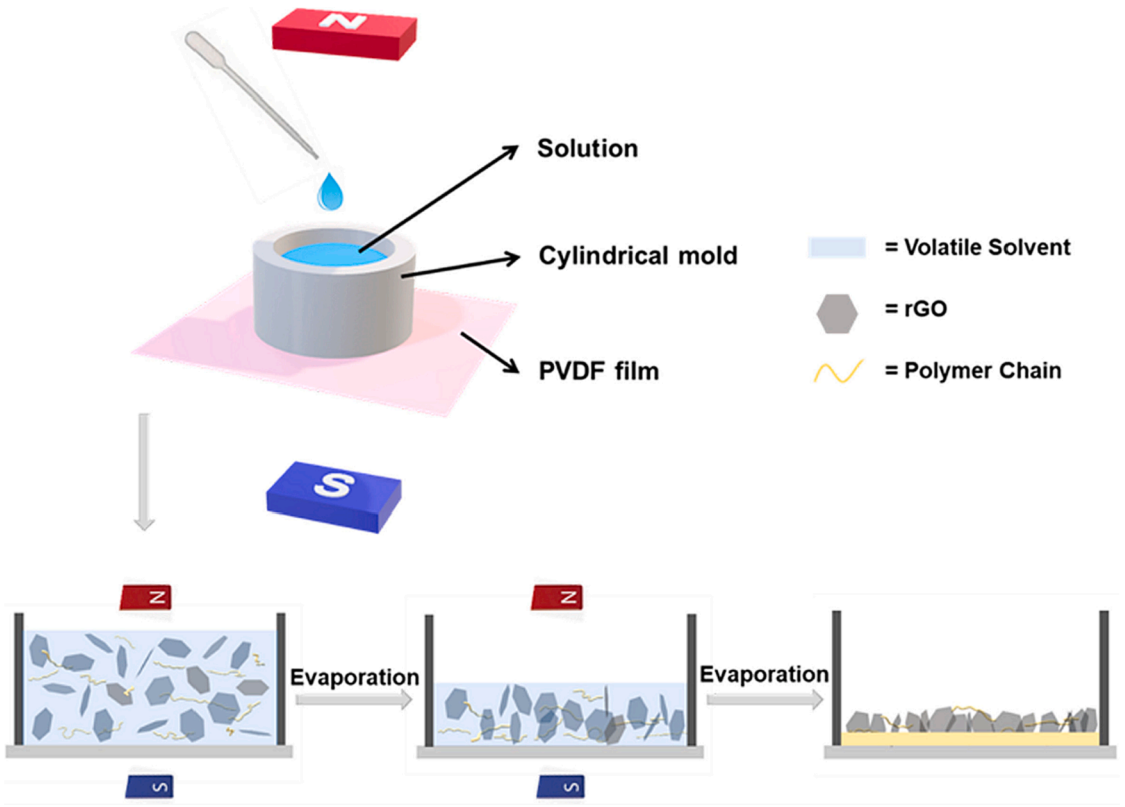

Fig. 13. Schematic showing the electrode preparation steps having vertically aligned graphene nanosheets in a static dual magnet system. Reproduced with permission [103]. Copyright 2021, Elsevier.

graphene sheets increase the capacitance as it can retain more ions due to higher wettability.

Tian et al. demonstrated graphene alignment without any Ferro/superparamagnetic particles under a magnetic field of 0.5 T produced by an electromagnet [35]. It is the first experimental proof that Landau diamagnetism prevails in graphene nanosheets under a magnetic field. Moreover, graphene orientation at different angles in N-methyl-pyrrolidone was further confirmed using a laser-light transmission system [35]. The results of several researchers, shown in Table 4, pave the way to orient diamagnetic large-size graphene sheets using ultra-high electromagnetic fields without ferro/superparamagnetic material.

Table 4
Graphene nanosheets aligned under an electromagnetic field and the potential application.

Product	Material/fillers	Magnetic Field Alignment	Composite Properties	Application	Reference
rGO + poly(3,4-ethylenedioxythiophene)	4:1 wt./wt. composite of rGO and polymer is fabricated under a magnetic field	12 T V	–	Supercapacitor	Lin et. al. (2021)[103]
GO added to polymer to form hydrogel composite	0.2 wt% GO are loaded to polymer for hydrogel fabrication	10 T V, H	–	–	Wu et. al. (2014)[140]
GO added to HEMA polymer to form a 300 μm thin composite	GO is photocrosslinked using UV in HEMA under magnetic field	6 T V, H	Vertically aligned composite showed enhanced antibacterial activity	Antibacterial activity	Lu et. al. (2017)[108]
GNPs are added to PDMS under magnetic field	3 wt% GNPs are added in PDMS and cured under a static magnetic field	10 T V, H	Aligned composite showed enhanced thermal conductivity of 174 % compared to pure PDMS	Thermal Conductivity	Li et. al. (2017)[142]
GO added to polymer for fabricating membrane	1 wt% GO is added and aligned in magnetic field	6 T V	Vertically aligned composite showed enhanced (71.7 %) antibacterial activity	Antibacterial activity	Lu et. al. (2018)[143]

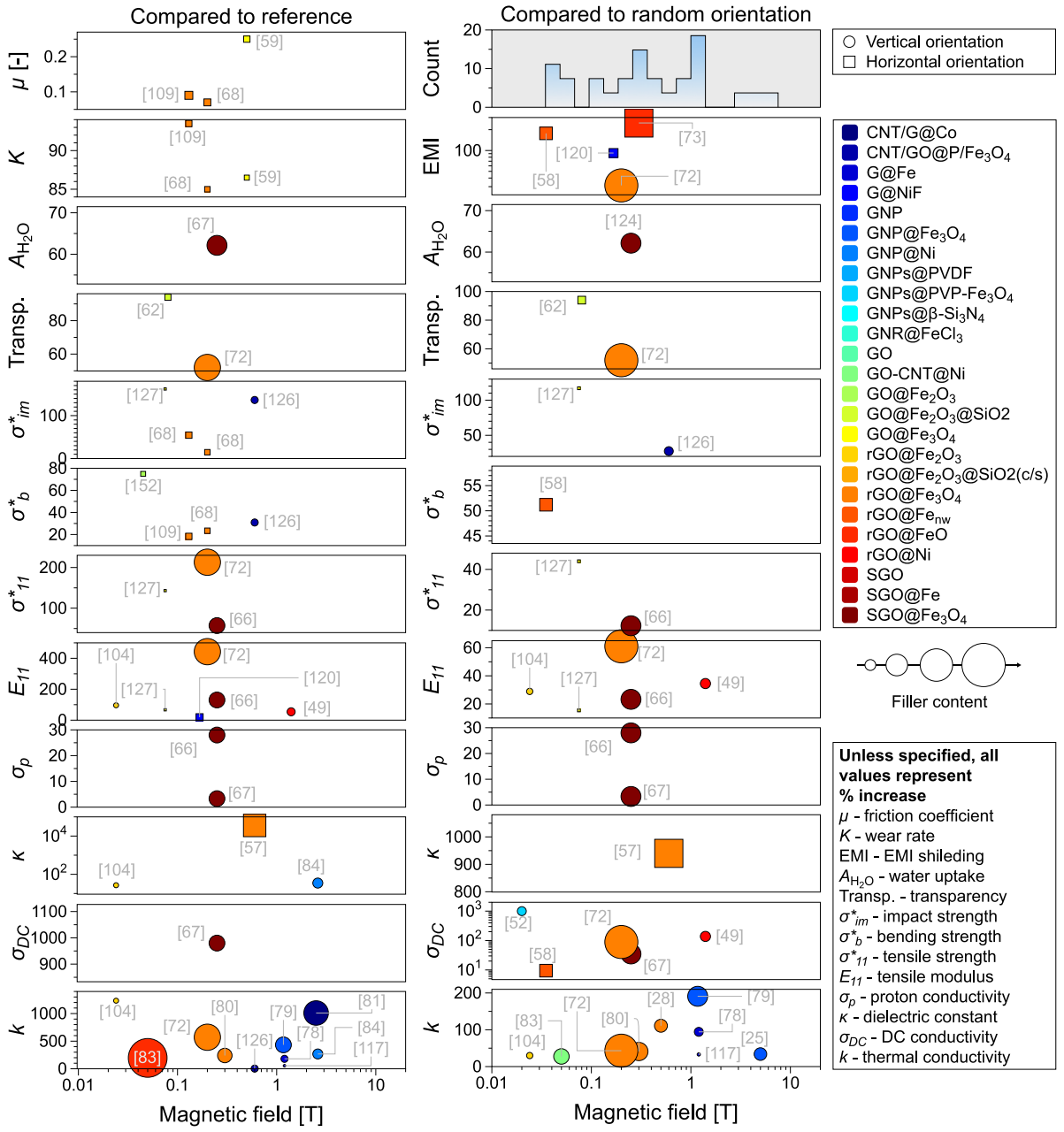

Fig. 14. Compilation of improvement in materials using magnetic fields, filler type, filler amount, vertical or horizontal alignment relative to the reference (left column) and relative to random orientation. Compared to Table 2, 3, 4, only material a property with at least two datapoints with respect to their reference or random orientation have been included. This effectively means that only studies using permanent magnets and magnetic nanoparticles could be included. The top graph on the right column represents a histogram of the magnetic field employed.

5. Trends, limitations, current challenges and future prospects

As illustrated in section 4.3, the use of magnetic fields for nanofiller inducing alignment in graphene-based systems remains a critical ingredient towards the goal of nanostructural control through field-filler interaction. The growing available body of literature on the topic shows significant potential for enhancing the performance of graphene-based nanocomposites for a broad range of applications. Fig. 14 summarizes the improvement of material properties with the help of magnetically induced graphene orientation therein. The improvement in performance is considerable both with respect to the reference (matrix material; left column in Fig. 14) or compared to random orientation, which is the standard morphology when preparing nanocomposites in the absence of orienting fields. The size of the symbols captures the amount of filler used fill color compiles all the types of graphenes used in the studies reviewed.

Several trends can be seen in the data compilation. Most experimental setups are concentrated in the 0.1–1.1 T range. For all applications, rGO and SGO based variations appear to dominate for experimental setups with magnetic fields below 1 T. Above 1 T the preferred fillers appear to be GNPs and G decorated with various magnetic nanoparticles as well as CNT hybrids. By far the most popular direct application of magnetically induced alignment seems to be for thermal management materials and mechanical properties. However, as the size of the datapoints indicates how much filler was used, large improvements in properties with the use of small quantities of standout not only in the case of thermal conductivity but also DC conductivity[66], proton conductivity[68], bending strength[62], transparency[75], wear rate[124] and friction coefficient.[71].

5.1. Limitations of current techniques

Permanent magnet and electromagnet systems, have shown so far impressive potential for the alignment of graphene nanosheets, leading to enhanced electric, thermal, mechanical, antibacterial, gas barrier and many more properties. However, current alignment techniques suffer from several limitations. When using a single-magnet system to align 2D materials, it has been observed that alignment is always poor due to the non-uniform magnetic field (Fig. 6).[104] The alignment can be improved with the use of a dual-magnet system which shows a more uniform magnetic field compared to a single-magnet system. However, even in the dual magnet system, the magnetic field strength varies drastically as the magnetic field lines are non-uniform, as shown in Fig. 6. Therefore, the graphene nanosheets in a composite fabricated using a dual magnetic system are still only partially unidirectionally aligned.[73].

In addition, there is a limitation on the size of magnets for producing a high magnetic field. A dual magnetic system made from rare earth materials is extremely expensive when producing a magnetic field of 10 T or more. Once the magnet is manufactured, it is very challenging to vary the strength of existing magnets. Therefore, a new magnet with the desired magnetic strength is always required, adding to the cost. Along with this, there is a huge challenge to attenuate the magnetic field around the magnet to protect humans and secure valuable instruments and materials, especially in an industrial setting. Furthermore, additional limitations are due to the manufacturing of the magnets themselves, as it is very difficult to obtain two similar magnets even with the same manufacturing method. Therefore, in such a case a dual magnet system could have an intrinsic small deviation in their magnetic field strength and pole positioning, which could cause misalignment of the magnetic field leading to partially aligned graphene nanosheets.

One of the major drawbacks of using a permanent magnet system compared to an electromagnet system is the operation of magnets in a high-temperature environment. The loss of strength of permanent magnets reduces their capability when working under high-temperature systems, therefore further reducing the number of applications it can be used in. Thermoplastic polymers as well as oven-cured thermoset polymers are thus more challenging to work with despite their extensive potential applications. While the electromagnets have the edge when working under high-temperature environments, they suffer from several other limitations compared to permanent magnets, such as a bulky electromagnetic core required to produce higher magnetic field strength, poor signal-to-noise ratio along with highly contaminated power line and switching noises, high amount of heat generation due to continuous current flow etc. Furthermore, a high-temperature generation leads to a a large variation in coil resistance. Therefore, a conventional electromagnet needs 30 min of warm-up time, with minor variations in power supply a high signal drift is observed and due to high power requirement for the generation of high strength magnetic field large number of electronic components are required which makes it bulky and therefore consumes large space [153]. Due to all these limitations, the use of permanent magnets is preferred by several researchers.

5.2. Current challenges

Several major challenges that could significantly impact the orientation of graphene nanosheets in magnetic fields can be readily identified:

- Reducing requirements on magnetic field strength

This is a major key technique performance indicator that can impact the performance of nano composites and their potential for implementation in large scale applications. As the intrinsic diamagnetic response of graphene becomes dominant at magnetic field strengths of 9 T or more, most studies have focused on doping of graphene with superparamagnetic nanoparticles. However, there are three major factors limiting their use. Firstly, their insertion into the graphene lattice may affect graphene's electrical conductivity, mechanical strength, etc., thus effectively limiting the performance of graphene-based devices. Secondly, achieving a homogeneous distribution of superparamagnetic nanoparticles on the graphene surface remains a challenge. Non-uniform doping can result in spatial variations in the magnetic response and orientation of the graphene, leading to inconsistencies in nanocomposite performance. And finally, superparamagnetic nanoparticles tend to agglomerate over time. Therefore, more research is required to find ways to counter these issues, along with finding new methods to introduce paramagnetism in graphene to control it at low magnetic fields.

- Magnetic field uniformity in permanent magnet setups

While the magnetic orientation setups reviewed can generate sufficiently strong magnetic fields for achieving orientation, they often lack in magnetic field uniformity. This is a major drawback especially for aligning graphene over larger material volumes. Consequently, the alignment achieved using such setups tends to be imperfect and inconsistent, hindering overall improvements in material properties. This would also negatively impact upscaling efforts. While determining the uniformity of magnetic fields

experimentally could be a rather difficult task, modeling the magnetic fields, especially in magnetostatic conditions, could readily accompany experimental investigations.

- Magnetic fields at high temperatures

Enabling magnetic fields for orientation at high temperatures could vastly increase the potential of all alignment techniques presented in terms of matrix materials and consequently potential for industrial applications. Specifically, the ability to orient graphene in the proximity of high temperatures is required to induce orientation in molten polymers. Currently, aligning graphene under a magnetic field at high temperatures can affect the strength and uniformity of the applied magnetic field. Thermal fluctuations can disrupt the alignment process and lead to inconsistent results. Moreover, high temperatures might induce eddy currents in the sample, which can generate their own magnetic fields and interfere with the alignment. As the temperature increases, the mobility of graphene atoms and the surrounding matrix material also rises. This increased mobility can make it challenging to maintain the alignment induced by a magnetic field. In addition, elevated temperatures can accelerate oxidation and contamination processes. Graphene is highly susceptible to oxidation, especially in the presence of oxygen or water vapor. These reactions can modify the graphene structure and compromise its properties, including alignment.

- Combining magnetic fields with flow-fields

From a manufacturing point of view, flow-based structuring of materials constitutes well established and highly productive methods. However, inducing filler orientation in a direction other than the flow direction can be a challenge for many applications. At the same time, magnetic field orientation setups are constrained in terms of scalability, both in terms of size as well as productivity. Thus, combining magnetic and flow fields could be a solution to compensate for their respective disadvantages.

- Tailoring materials for optimal orientation conditions

Although rarely reported, the rheological properties of graphene-filled matrix materials play a pivotal role in precisely controlling the orientation of nanoparticles when subjected to a magnetic field. Ideally the rheological properties of the test fluids should enable quick orientation under a magnetic field while once oriented the structure should be as arrested preventing de-orientation such that for example a curing system could be further moved into an oven for complete curing. Thus, for example, in reactive systems such as epoxy, coupling curing kinetics to rheological properties and orientation dynamics would be essential for a precise and repeatable control of the alignment process. While represented in section 3.1 solely by a Newtonian shear viscosity, when it comes to the micro-hydrodynamics of particles, it is known that in many cases considering a pure viscous (Newtonian) fluid cannot account for all effects [94].

To conclude, the alignment of graphene in a magnetic field, with and without the use of magnetic nanoparticles, holds significant potential for a wide range of applications. The ability to manipulate graphene's properties through alignment opens up new opportunities in electronics, energy storage, and biomedical engineering. Several major challenges have been identified and it is expected that with new advances in those key aspects novel applications could be explored, integrating aligned graphene with other materials, combining magnetic with e.g., flow and deepening our understanding of the underlying physics. We can expect significant advancements in this field, leading to the development of innovative technologies with transformative societal impact.

CRediT authorship contribution statement

Viney Ghai: Conceptualization, Methodology, Data curation, Visualization, Writing - original draft, Writing - review & editing. **Sajjad Pashazadeh:** writing - original draft, writing - review & editing. **Hengzhi Ruan:** Visualization. **Roland Kádár:** Conceptualization, Visualization, Writing - original draft, Writing - review & editing, Supervision.

Declaration of competing interest

The authors declare that they have no known competing financial interests or personal relationships that could have appeared to influence the work reported in this paper.

Data availability

Data will be made available on request.

Acknowledgements

VG and RG are grateful for the financial support of the 2D-TECH Vinnova competence centre (Ref. 2019-00068), Chalmers Area of Advance Materials Science, Chalmers Area of Advance Nano, and Chalmers Are of Advance Production. HR and RK are grateful for the financial support of the PEST-BIN project that has received funding from the European Union's Horizon 2020 Research and Innovation Programme under the Marie Skłodowska-Curie grant agreement No 955626. SP and RK are grateful for the financial support of Stora

Enso Oyj through the Biocomposite program founded by the Knut and Alice Wallenberg foundation (Dnr, KAW 2018.0451).

References

[1] Novoselov KS, Geim AK, Morozov SV, Jiang D, Zhang Y, Dubonos SV, et al. Science 1979;2004(306):666.
[2] Geim AK, Novoselov KS. Nat Mater 2007;6(3):183.
[3] Novoselov KS, Geim AK, Morozov SV, Jiang D, Katsnelson MI, Grigorieva IV, Dubonos SV, Firsov AA. Nature 2005;438(7065):7065.
[4] "ISO/TS 80004-13:2017(en), Nanotechnologies — Vocabulary — Part 13: Graphene and related two-dimensional (2D) materials," can be found under https://www.iso.org/obp/ui/#iso:std:iso:ts:80004:-13:ed-1:v1:en, **n.d.**
[5] Nakajima T, Matsuo Y. Carbon N Y 1994;32:469.
[6] Lerf A, He H, Forster M, Klinowski J. J Phys Chem B 1998;102:4477.
[7] Philos Trans R Soc Lond 1859;149:249.
[8] Hummers WS, Offeman RE. J Am Chem Soc 1958;80:1339.
[9] Wallace PR. P R W Ace 1947:71.
[10] Ferrari AC, Bonaccorso F, Fal'ko V, Novoselov KS, Roche S, Bøggild P, et al. Nanoscale 2015;7:4598.
[11] Tiwari SK, Sahoo S, Wang N, Huczko A. J Sci: Adv Mater Devices 2020;5:10.
[12] Avouris P, Dimitrakopoulos C. Mater Today 2012;15:86.
[13] Lee C, Wei X, Kysar JW, Hone J. Science 1979;2008(321):385.
[14] Wu X, Ding SJ, Lin K, Su J. J Mater Chem B 2017;5:3084.
[15] Savage N. Nature 2012;483(7389):S38.
[16] Nair RR, Blake P, Grigorenko AN, Novoselov KS, Booth TJ, Stauber T, et al. Science 1979;2008(320):1308.
[17] Wang F, Wang H, Mao J, **n.d.**, Doi: 10.1007/s10853-018-2849-4.
[18] Sierra-Romero A, Chen B. Nanocomposites 2018;4:137.
[19] Wu S, Peng S, Wang CH, 2018, Doi: 10.3390/polym10050542.
[20] Li X, Mckenna GB, Miquelard-Garnier G, Guinault A, Sollogoub C, Regnier G, et al. Polymer (Guildf) 2014;55:248.
[21] Pandit S, Gaska K, Mokkapati VRSS, Celauro E, Derouiche A, Forsberg S, et al. Small 2020:16. https://doi.org/10.1002/SMLL.201904756.
[22] Yu WC, Xu JZ, Wang ZG, Huang YF, Yin HM, Xu L, et al. Compos Part A Appl Sci Manuf 2018;110:237.
[23] Lacey SD, Kirsch DJ, Li Y, Morgenstern JT, Zarket BC, Yao Y, et al. Adv Mater 2018;30:1705651.
[24] Zhang K, Li X, Nie M, Wang Q. Compos Sci Technol 2018;158:121.
[25] Kim JE, Han TH, Lee SH, Kim JY, Ahn CW, Yun JM, et al. Angew Chem Int Ed 2011;50:3043.
[26] Shen X, Zheng Q, Kim JK. Prog Mater Sci 2021;115:100708.
[27] Yakovenko O, Matzui L, Danylova G, Zadorozhnii V, Vovchenko L, Perets Y, et al. Nanoscale Res Lett 2017;12:1.
[28] Yan H, Wang R, Li Y, Long W. J Electronic Mater 2014;44(2):658.
[29] He H, Guan L, Le Ferrand H. J Mater Chem A Mater 2022;10:19129.
[30] Griffin A, Guo Y, Hu Z, Zhang J, Chen Y, Qiang Z. Polym Compos 2022;43:5747.
[31] Lei C, Xie Z, Wu K, Fu Q, Lei C, Xie Z, et al. Adv Mater 2021;33:2103495.
[32] Zhang Z, Qu J, Feng Y, Feng W. Compos Commun 2018;9:33.
[33] J. D. 1925-2016 Jackson, **n.d.**
[34] Tang T, Tang N, Zheng Y, Wan X, Liu Y, Liu F, Xu Q, Du Y. Sci Rep 2015;5(1):1.
[35] Tian B, Lin W, Zhuang P, Li J, mo Shih T, Cai W. Carbon N Y 2018;131:66.
[36] Takahashi T, Sado M, Sugimoto N, Tatami J, Iijima M, Inagaki S, et al. Adv Powder Technol 2005;2016:27.
[37] Heremans J, Olk CH, Morelli DT. Phys Rev B 1994;49:15122.
[38] Shulman D, Lewkowicz M, Bormashenko E. J Magn Magn Mater 2023;571:170553.
[39] Popov IA, Bozhenko KV, Boldyrev AI. Nano Res 2012;117.
[40] Zagaynova V. Carbon-Based Magnetic Nanomaterials, Doctoral Thesis, Umeå University, Sweden, n.d.
[41] Chen L, Guo L, Li Z, Zhang H, Lin J, Huang J, Jin S, Chen X. Sci Rep 2013;3(1):1.
[42] Sepioni M, Nair RR, Rablen S, Narayanan J, Tuna F, Winpenny R, et al. Phys Rev Lett 2010;105:207205.
[43] He H, Gao C. ACS Appl Mater Interfaces 2010;2:3201.
[44] Wang Y, Hoang Y, Song Y, Zhang X, Ma Y, Liang J, et al. Nano Lett 2009;9:220.
[45] He L, Li M, Xu H, Hu B. Nanoscale 2017;9:2563.
[46] Yang L, Cohen ML, Louie SG. Phys Rev Lett 2008;101:186401.
[47] Kimura T. Polym J 2003;35(11):23.
[48] Geng J, Men Y, Liu C, Ge X, Yuan C. RSC Adv 2021;11:16592.
[49] Yoonessi M, Gaier JR, Peck JA, Meador MA. Carbon N Y 2015;84:375.
[50] Xu H, Prabhakaran P, Kim SH, Jung J, Narayan R, Kim SO, et al. J Phys Chem C 2018;122:6912.
[51] Erb RM, Segmehl J, Charilaou M, Löffler JF, Studart AR. Soft Matter 2012;8:7604.
[52] Wu S, Zhang J, Ladani RB, Ghorbani K, Mouritz AP, Kinloch AJ, et al. Polymer (Guildf) 2016;97:273.
[53] Huang Y, fa Xiao C, lin Huang Q, liang Liu H, qiang Hao J, Song L. J Memb Sci 2018;548:184.
[54] Magaye R, Zhao J, Bowman L, Ding M. Exp Ther Med 2012;4:551.
[55] Ma D, Su Y, Tian T, Yin H, Zou C, Huo T, et al. ACS Appl Mater Interfaces 2020;12:37418.
[56] Shemshadi R, Khodayari S, Ghafarian SR, Gorji M. Polymer-Plastics TechnolMater 2020;59:204.
[57] Ding L, Liu L, Li P, Lv F, Tong W, Zhang Y. J Appl Polym Sci 2016;133. https://doi.org/10.1002/APP.43041.
[58] Fu P, Huan X, Luo J, Ren S, Jia X, Yang X. ACS Appl Nano Mater 2020;3:9340.
[59] Bai T, Liu Z, Pei Z, Fang W, Ma Y. ACS Omega 2021;6:9243.
[60] Zhang D, Yang F, Wang R. Appl Phys A Mater Sci Process 2022;128. https://doi.org/10.1007/S00339-022-05324-3.
[61] Goei R, Nguyen TD, Zhang X, Ong AJ, Mandler D, Magdassi S, et al. Eur Phys J: Special Topics 2022. https://doi.org/10.1140/EPJS/S11734-022-00543-4.
[62] Lei Y, Zhang X, Liu Q, Tao Y, Sun Y, You B. Prog Org Coat 2022;173. https://doi.org/10.1016/J.PORGCOAT.2022.107184.
[63] Lin JS, Ma WT, Shih CM, Yu BC, Teng LW, Wang YC, Cheng KW, Chiu FC, Lue SJ. Energies (Basel) 2016;1:9. https://doi.org/10.3390/EN9121003.
[64] Zhu W, Qin Y, Wang Z, Zhang J, Guo R, Li X. J Energy Chem 2019;31:1.
[65] Park O-K, Tiwary CS, Yang Y, Bhowmick S, Vinod S, Zhang Q, et al. Nanoscale 2017;9:6991.
[66] Beydaghi H, Javanbakht M. Ind Eng Chem Res 2015;54:7028.
[67] Vinothkannan M, Kim AR, Gnana Kumar G, Yoon JM, Yoo DJ. RSC Adv 2017;7:39034.
[68] Liu C, Yan H, Chen Z, Yuan L, Liu T. J Mater Chem A Mater 2015;3:10559.
[69] Ren PG, Wang H, Yan DX, Huang HD, Bin Wang H, Zhang ZP, et al. Compos Part A Appl Sci Manuf 2017;97:1.
[70] Le Ferrand H, Bolisetty S, Demirörs AF, Libanori R, Studart AR, Mezzenga R. Nat Commun 2016;7(1):1.
[71] Dai M, Zhai Y, Wu L, Zhang Y. Carbon N Y 2019;152:661.
[72] Li H, Hu J, Liang Y, Jiang G. ACS Sustain Chem Eng 2022;2022:16377.
[73] Hong SY, Kim YC, Wang M, Do Nam J, Suhr J. Eur Polym J 2020;127. https://doi.org/10.1016/J.EURPOLYMJ.2020.109595.

[74] Santhosh M, Choi JH, Choi JW. Nanomaterials 2019:9. https://doi.org/10.3390/NANO9091293.
[75] Wu Q. Mater Lett 2022;321:132370.
[76] Dong S, Chen S, Li B, Wang X. J Intell Mater Syst Struct 2021;32:1377.
[77] Younes H, Kuang X, Lou D, DeVries B, Rahman MM, Hong H. Mater Res Bull 2022;154. https://doi.org/10.1016/J.MATERRESBULL.2022.111938.
[78] Renteria J, Legedza S, Salgado R, Balandin MP, Ramirez S, Saadah M, et al. Mater Des 2015;88:214.
[79] Shi Y, Ma W, Wu L, Hu D, Mo J, Yang B, et al. J Appl Polym Sci 2019;136. https://doi.org/10.1002/APP.47951.
[80] Yan H, Tang Y, Long W, Li Y. J Mater Sci 2014;49:5256.
[81] Li X, Li Y, Alam MM, Chen P, Xia R, Wu B, et al. RSC Adv 2020;10:3357.
[82] Xu J, Wang R, Jiang H, Liu X, An L, Jin S, et al. Adv Sci 2021:8. https://doi.org/10.1002/ADVS.202102477.
[83] Hu C, Zhang H, Neate N, Fay M, Hou X, Grant D, Xu F. Polymers 2022;14:58.
[84] Yang B, Jia N, Wang X, Pan Y, Luo M, Chen X, et al. Macromol Mater Eng 2022:2200144.
[85] Hong J, Niyogi S, Bekyarova E, Itkis ME, Ramesh P, Amos N, et al. Small 2011;7:1175.
[86] Lin F, Zhu Z, Zhou X, Qiu W, Niu C, Hu J, et al. Adv Mater 2017:29. https://doi.org/10.1002/ADMA.201604453.
[87] Yazyev OV. Rep Prog Phys 2010;73:056501.
[88] Kan E, Li Z, Yang J, 2011; 3: 433, https://doi.org/10.1142/S1793292008001350.
[89] Sheka EF, Popova N, Popova V. Phys Usp 2018;61:645.
[90] Rao CNR, Matte HSSR, Subrahmanyam KS, Maitra U. Chem Sci 2011;3:45.
[91] Li Z, Li S, Xu Y, Tang N. Chem Commun 2023. https://doi.org/10.1039/D3CC01311A.
[92] Erb RM, Libanori R, Rothfuchs N, Studart AR. Science 1979;2012(335):199.
[93] Barthès-Biesel D. Microhydrodynamics and Complex Fluids 2012:1.
[94] Graham MD. Microhydrodynamics, Brownian Motion, and Complex Fluids 2018; 1.
[95] Bretherton FP. J Fluid Mech 1962;14:284.
[96] Kim Sangtae, Karrila SJ. Microhydrodynamics : Principles and Selected Applications. Dover Publications; 2013.
[97] Perrin F. J Phys Radium 1934;5:497.
[98] Liu L, Li X, Liu Z, Zhang S, Qian L, Chen Z, et al. J Memb Sci 2022;653:120516.
[99] Pan G, Hu L, Zhang F, Chen Q. J Phys Chem Lett 2021;12:3476.
[100] Billaud J, Bouville F, Magrini T, Villevieille C, Studart AR. Nat Energy 2016;1(8):1.
[101] Kao KC. Br J Appl Phys 1961;12:629.
[102] Ominato Y, Koshino M. Phys Rev B 2013;87:115433.
[103] Lin S, Tang J, Zhang K, Suzuki TS, Wei Q, Mukaida M, et al. J Power Sources 2021;482. https://doi.org/10.1016/J.JPOWSOUR.2020.228995.
[104] Liu D, Chi H, Ma C, Song M, Zhang P, Dai P. Compos Sci Technol 2022;220:109292.
[105] Lin F, Yang G, Niu C, Wang Y, Zhu Z, Luo H, et al. Adv Funct Mater 2018:28. https://doi.org/10.1002/ADFM.201805255.
[106] Zhang L, Zeng M, Liu Z, Ma Q, Lu Y, Ma J, et al. ACS Appl Energy Mater 2021;4:5590.
[107] Zhang L, Zeng M, Wu D, Yan X. ACS Sustain Chem Eng 2019;7:6152.
[108] Lu X, Feng X, Werber JR, Chu C, Zucker I, Kim JH, et al. Proc Natl Acad Sci U S A 2017;114:E9793.
[109] Liu C, Yan H, Lv Q, Li S, Niu S. Carbon N Y 2016;102:145.
[110] Tong M, Cao J, Chen X, Zhang H, Wu W, Ma H. RSC Adv 2019;9:19457.
[111] Cheon Youn S, Woo Kim D, Bo Yang S, Mi Cho H, Hyun Lee J, Jung HT. Chem Commun 2011;47:5211.
[112] Shen J, Zhu Y, Zhou K, Yang X, Li C. J Mater Chem 2012;22:545.
[113] Genorio B, Peng Z, Lu W, Price Hoelscher BK, Novosel B, Tour JM. ACS Nano 2012;6:10396.
[114] Zhang H, Wu W, Zhou J, Zhang X, Zhu T, Tong M. Cellul 2021;28:2303.
[115] Jiang Z, Li J, Aslan H, Li Q, Li Y, Chen M, et al. J Mater Chem A Mater 2014;2:6714.
[116] Zou C, Hu J, Su Y, Zhou Z, Cai B, Tao Z, et al. Sens Actuators B Chem 2020;306:127546.
[117] Wu Z, Chen J, Li Q, Xia DH, Deng Y, Zhang Y, et al. Materials 2021:14. https://doi.org/10.3390/MA14082013.
[118] Xu B, Mao N, Zhao Y, Tong L, Zhang J. J Phys Chem Lett 2021;12:7442.
[119] Heon Ryu J, Mi Yang S, Uk Lee J, Ho Kim J, Jae Yang S. Carbon Lett 2022;1:3.
[120] Babu RD, Rahaman A, Sharma SMSD, Bose S, P ST. J Inorg Organomet Polym Mater 2022;32:4077.
[121] Zhu W, Jiang G, Xu L, Li B, Cai Q, Jiang H, et al. Anal Chim Acta 2015;886:37.
[122] Ma WT, Kumar SR, Hsu CT, Shih CM, Tsai SW, Yang CC, et al. J Memb Sci 2018;563:259.
[123] He J, Wang H, Qu Q, Su Z, Qin T, Tian X. Compos Part A Appl Sci Manuf 2020;139. https://doi.org/10.1016/J.COMPOSITESA.2020.106062.
[124] Rodríguez-Serradet A, Ciftci S, Mikosch A, Kuehne AJC, De Melo CP, Cao-Milán R. RSC Adv 2016;6:94256.
[125] Yuwawech K, Wootthikanokkhan J, Tanpichai S. Mater Today Proc 2020;23:703.
[126] Yao D, Peng N, Zheng Y. Compos Sci Technol 2018;167:234.
[127] Chaichi M, Sharif F, Mazinani S. J Mater Sci 2018;53:5051.
[128] Antman-Passig M, Shefi O. Nano Lett 2016;16:2567.
[129] Kukhta AV, Kuzhir PP, Maksimenko SA, Vorobyova SA, Kukhta IN, Pochtenny AE, et al. Prog Org Coat 2019;137. https://doi.org/10.1016/J.PORGCOAT.2019.105366.
[130] Li J, Pei Q, Wang R, Zhou Y, Zhang Z, Cao Q, et al. DOI 2018. https://doi.org/10.1021/acsnano.7b08770.
[131] Yin S, Zhang T, Yu Y, Bu X, Zhang Z, Geng J, et al. Materials 2023;16:476.
[132] Zheng K, Li K, Chang TH, Xie J, Chen PY. Adv Funct Mater 2019:29. https://doi.org/10.1002/ADFM.201904603.
[133] Wang X, Lv J, Ding R, jiang Gui T, Sun ML. Int J Electrochem Sci 2020;15:4089.
[134] Yin S, Wang J, Li Y, Wu T, Song L, Zhu Y, et al. Electroanalysis 2021;33:2216.
[135] Liu Y, Lu M, Wu K, Yao S, Du X, Chen G, et al. Compos Sci Technol 2019;174:1.
[136] Ding R, Chen S, Zhou N, Zheng Y, Jun Li B, jiang Gui T, Wang X, hua Li W, bin Yu H, wen Tian H. J Alloys Compd 2019;784:756.
[137] Shen XJ, Dang CY, Tang BL, Yang XH, Nie HJ, Lu JJ, et al. Mater Des 2020;185. https://doi.org/10.1016/J.MATDES.2019.108257.
[138] Li D, Liu Y, Ma H, Wang Y, Wang L, Xie Z. RSC Adv 2015;5:31670.
[139] Su S, Pan G, Xiao X, Wang Q, Zhang F. Appl Phys Lett 2020;117. https://doi.org/10.1063/5.0006234.
[140] Wu L, Ohtani M, Takata M, Saeki A, Seki S, Ishida Y, et al. ACS Nano 2014;8:4640.
[141] Matsumoto M, Saito Y, Park C, Fukushima T, Aida T. Nat Chem 2015;7:730.
[142] Li B, Dong S, Wu X, Wang C, Wang X, Fang J. Compos Sci Technol 2017;147:52.
[143] Lu X, Feng X, Zhang X, Chukwu MN, Osuji CO, Elimelech M. Environ Sci Technol Lett 2018;5:614.
[144] Lu KC, Wang JK, Lin DH, Chen X, Yin SY, Chen GS. Anal Methods 2020;12:2661.
[145] Zhou C, Lin F, Tang Y, Liu Y, Luo X, Qi Y, et al. Mater Today Phys 2023;31:100985.
[146] Smarzewska S, Miękoś E, Guziejewski D, Zieliński M, Burnat B. Anal Chim Acta 2018;1011:35.
[147] Li X, Lin D, Lu K, Chen X, Yin S, Li Y, et al. Anal Chim Acta 2020;1122:31.
[148] Bie L, Wang J, Yan G, Xie D, Jia Y, Chen S, et al. Liq Cryst 2020;48:368.
[149] Lin F, Niu C, Hu J, Wang Z, Bao J. IEEE Nanotechnol Mag 2020;14:14.
[150] Niu C, Lin F, Wang ZM, Bao J, Hu J. J Appl Phys 2018;123. https://doi.org/10.1063/1.5005539.

[151] Dyer C, Gkaliou K, Anderson P, Harrison C, Eaton M, Hall J. Int J Appl Electromagn Mech 2019;61:S23.
[152] Liu S, Chen Y, Li X, Wang L, Du H. Constr Build Mater 2023;369:130545.
[153] Nair SS, Vinodkumar V, Sreedevi V, Nagesh DS. Med Biol Eng Comput 2015;53:1187.